ALMA MATER STUDIORUM – UNIVERSITÀ DI BOLOGNA

SCUOLA DI INGEGNERIA E ARCHITETTURA
Dipartimento di Ingegneria dell'Energia Elettrica e dell'Informazione
«Guglielmo Marconi»
-DEI-

MASTER DEGREE
IN
TELECOMMUNICATIONS ENGINEERING

Thesis on
Optical Fiber Systems M

INVESTIGATION ON THE POLARIZATION DEPENDENT LOSS IN THE RADIO-OVER-FIBER SYSTEMS USED FOR THE SQUARE KILOMETER ARRAY RADIO TELESCOPE

Candidate:
Vittorio Di Paolo

Supervisor:
Prof. **Giovanni Tartarini**

Cosupervisors:
Eng. **Jacopo Nanni**
Eng. **Federico Perini**

Accademic Year
2021/2022

Session III

Abstract

The Square Kilometer Array-low (SKA-low) system requirements for high sensitivity and dynamic range are met in large part by the signal reception chain. The choice of architecture and receiver system design for SKA-low is influenced by the trade-off between gain, linearity, and low power consumption as well as cost, high reliability, robustness under extreme environments, and finally, the distance between the antennas and the acquisition systems. RF-over-fiber systems have been chosen as the technology for the SKA-low RF signal conveyance. Together with explanations of the creation of the receiver prototypes, the selection's justifications are presented. At the chosen SKA-low site in Western Australia, the prototypes were set up and put on demonstrator arrays.

The thermal characterization of the receiver system has received particular focus, especially when both the optical medium and the transmitting component are subject to fluctuations in the ambient outside temperature.

For this reason, particular emphasis has been placed on the analysis of optical receivers, both those currently used in AAVS2 and those that will be used for in the future for AAVS3. Finally, several simulations were conducted using software developed to describe the behavior of signals received following propagation through RF-over-fiber systems under certain environmental conditions.

SUMMARY

Chapter 1

SKAO (Square Kilometre Array Observatory) is an international collaboration aimed to design, build and operate the world's largest and most powerful radio telescope once completed. The project is currently being built in South Africa and Australia, and it will consist of thousands of dishes and antennas spread over thousands of kilometers.
These telescopes will operate at different frequencies and are named accordingly. SKA-Mid comprises of 197 traditional dish antennas, while SKA-Low comprises of 131,072 smaller tree-like antennas.

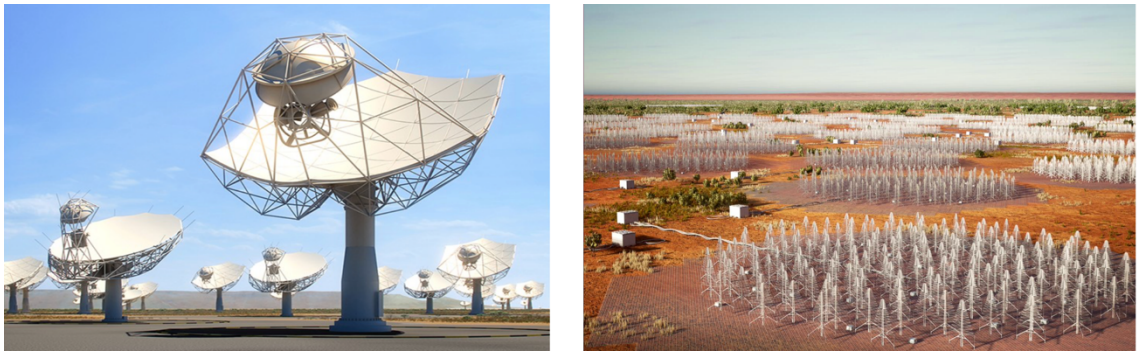

Figure1 on left SKA-mid dish antennas, on right SKA-low tree-like antennas.

Both arrays will be spread across large distances, with the farthest antennas separated by 150km in South Africa and 65km in Australia.
Cutting-edge technology, including some of the fastest supercomputers globally, will enable the telescopes to scrutinize the Universe in detail, uncovering the inner workings of galaxies and aiding in the comprehension of the extreme environments surrounding black holes. Moreover, the telescopes will track the movements of gravitational waves and facilitate a myriad of other ambitious scientific investigations[1].
The decision to establish the SKA telescopes in South Africa and Western Australia was based on the radio quietness of the locations, which is a vital consideration for conducting precise and accurate radio astronomy measurements. The SKA-Mid site in South Africa is located within the Karoo Central Astronomy Advantage Area, whereas the SKA-Low site in Western Australia is situated within CSIRO's Murchison Radio-astronomy Observatory, which is located on the traditional lands of the Wajarri Yamaji. These areas were carefully chosen for their low levels of radio frequency interference (RFI), allowing

the telescopes to operate with maximum sensitivity and precision. This strategic placement of the telescopes will significantly enhance our understanding of the Universe and enable groundbreaking scientific discoveries.

RFI generated by the SKA telescopes will be kept to a minimum and will be managed as much as feasible by the infrastructure. This also means that every structure on site that will contain computing equipment will be completely protected to prevent interference with observations.

1.1 Introduction to SKA-low

SKA-low is the component of the SKAO project that focuses on low frequency observations. It will be in Western Australia (Murchison Shire), and it will consist of 131,072 of log-periodic antennas spread over an area of around 65 square kilometers. The goal of SKA-low is to observe the universe at frequencies ranging from 50 MHz to 350 MHz, and it allows the astronomers to study a wide range of phenomena, from the early universe to the formation of galaxies and the evolution of black holes.

Radio over Fiber (RFoF) technology will play an important role in SKA-low, particularly in the transmission of the vast amounts of signals generated by the telescope's thousands of antennas. RFoF technology enables the transmission of radio signals over optical fiber, allowing for long-distance data transfer with minimal signal loss.

In SKA-low, RFoF technology is expected to be used to transport the signals from the telescope's antennas to a central processing facility, where the data will be processed and analyzed. This will require the development of specialized RFoF systems capable of handling complex signal processing requirements of the SKA-low project.

The challenging environmental conditions and limited infrastructure at the SKA-low site have led to the decision to have a single central processing facility (CPF) and a small number of remote processing facilities (RPFs) that will be directly connected to 60% and 40% of the antennas, respectively. To ensure high-fidelity delivery of the radioastronomical signals over distances ranging from 500m to a few kilometers, optical fiber is the only viable transmission channel. As a result, the radioastronomical signals from the 512 array stations, each consisting of 256 double polarization antennas (512x256=131,072 tree-like antennas), will be connected to the CPF or RPFs using RFoF-based links in the final design of SKA-low.

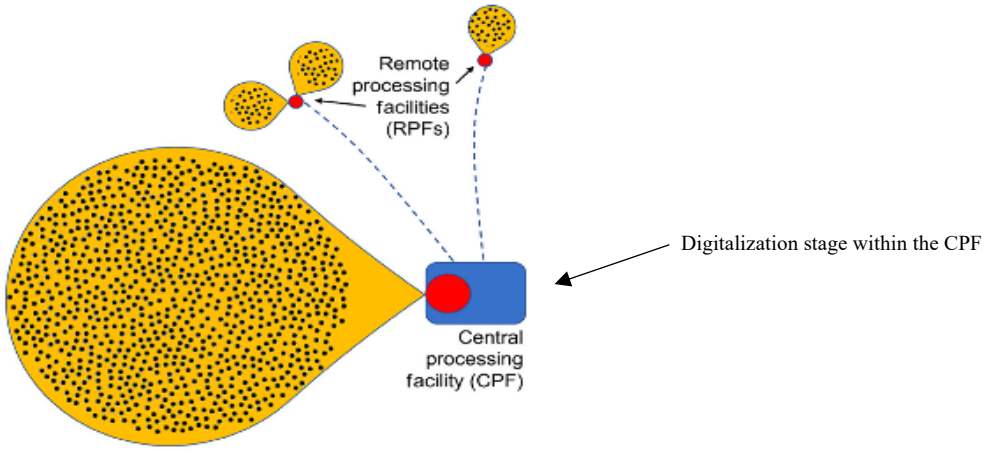

Figure 1.1 typical SKA-low site.

The design of the RFoF receiver for use in SKA-low has undergone several refinement operations, leading to the current finalized structure. This design process was aided by the creation of demonstrator stations, including the Aperture Array Verification System (AAVS1 and AAVS2 and forthcoming AAVS3) located at the Murchison Radio-astronomy Observatory (MRO) near the SKA-low site. Each demonstrator station consists of 256 double polarization antennas, with SKA log periodic antennas (SKALA2 and SKALA4.1) used for AAVS systems. These stations are connected to a shielded room borrowed from the Australian Square Kilometer Array Pathfinder (ASKAP) facility via RFoF-based links with a length of approximately 5.5 km. In the shielded room, all the CPF functionalities are carried out[2].

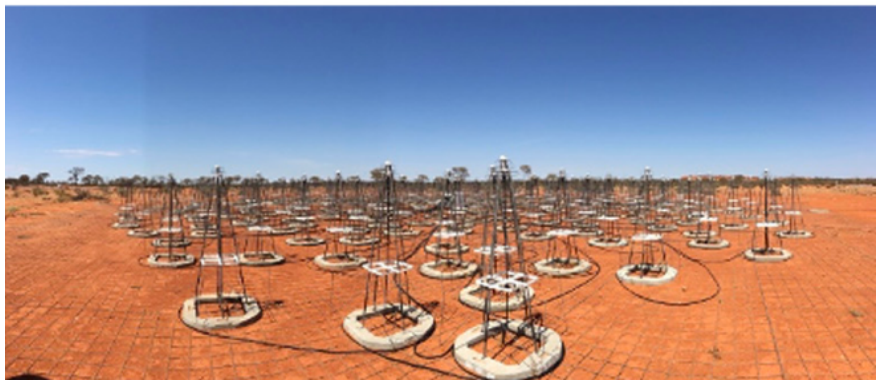

Figure 1.1.*2 AAVS1 prototype stations deployed at the MRO*.

Figure 1.1.3 *AAVS2 prototype stations deployed at the MRO.*

1.2 SKA-low receiver

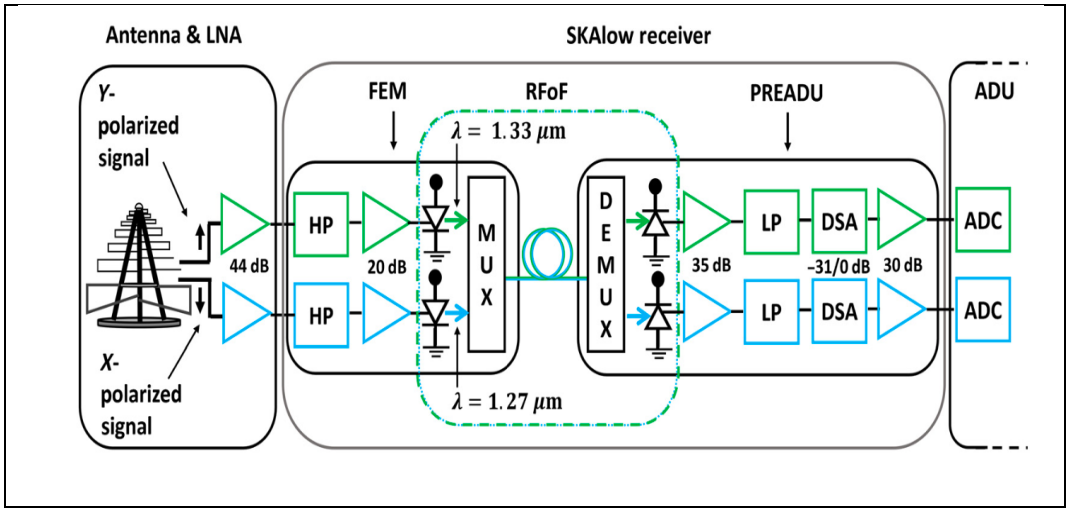

Figure 1.2

In Figure 1.2 the entire SKAlow system is reported; as is possible to see, it is the link in between the antennas of the site and the station digital processing system located onto RPFs or CPFs.

The analogue receiver is divided into three main parts: the RF/optical transmitter, called Front End Module (FEM), the optical fiber, and the optical/RF receiver, called pre-Analogue to Digital unit (PREADU). The RFoF link is completely embedded in the RF analogue receiver chain since its active components, the WDM (Wave Division Multiplex) LASER sources and the WDM double PD (photodiodes), are parts of the FEM and PREADU circuits, respectively.

1.2.1 WDM for SKAlow

In fiber optic communication systems, WDM technique is commonly employed to enable the transmission of multiple signals through the same optical fiber simultaneously. This is achieved by using distinct optical carriers that are modulated with different signals at different wavelengths. These signals do not interfere with each other during transmission and can be readily separated into their individual components at the receiver end through demultiplexing.

In the SKA-low scenario, the received radio-astronomical signal from the field is transmitted using two wavelengths that are multiplexed, whose correspond to the horizontal and vertical polarizations of the antenna signals.

In this case of study, the wavelengths of 1270 nm and 1330 nm were selected due to their favorable optical attenuation characteristics, while also minimizing the occurrence of strong phase errors across multiple km-range optical links transmitting the same wavelength (due to the chromatic dispersion effect).

The term BOSA is frequently used to describe the WDM optical components utilized in RFoF links. BOSA is an acronym for Bidirectional Optical Sub Assembly, which refers to a package that contains both a LASER source (DFB LASER is used because of lower noise and distortion performances) for transmitting optical signals and a photodiode for receiving them within the same assembly.

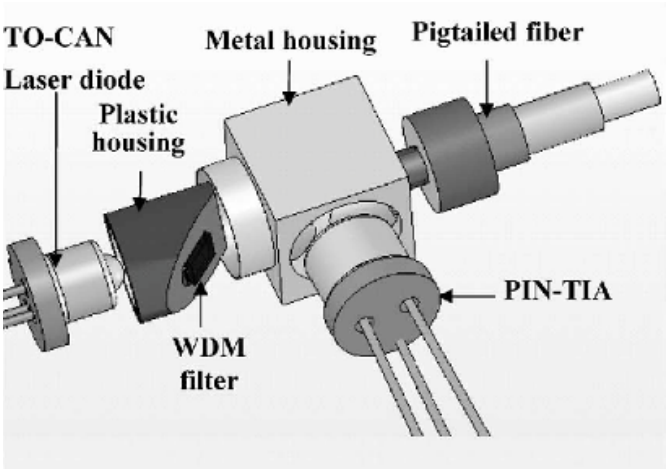

Figure 1.2.1 BOSA architecture.

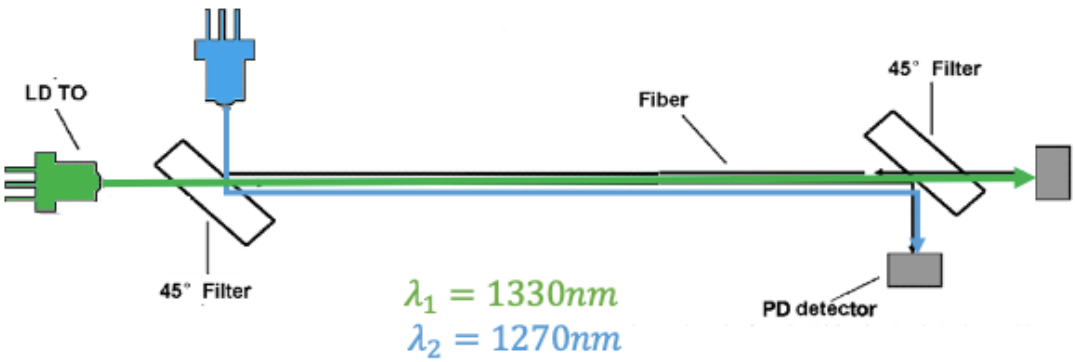

Figure 1.2.2 (a): ***Block diagram***

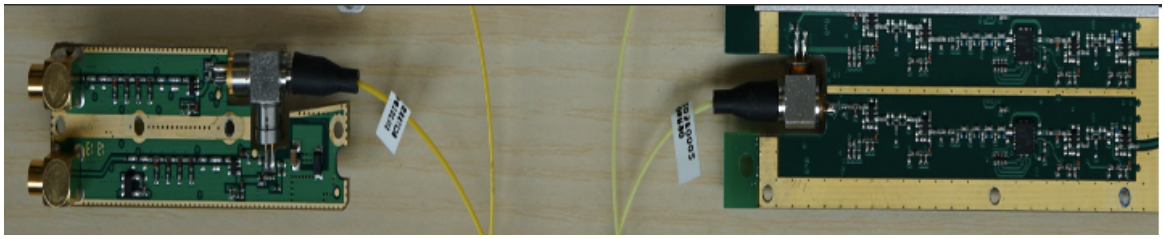

Figure 1.2.2 (b)

Figures 1.2.2 (a) and (b) represent the final optical configuration selected for SKAlow and all its demonstrators since AAVS1. Furthermore in (a) is possible to appreciate how, at both link ends, a 45° WMD thin film filter is utilized[3].

1.3 Impairments due to Polarization Dependent Loss and Polarized mode dispersion combined effects

In March of 2020, unusual fluctuations in the levels of optical received powers for both optical wavelengths were detected and analyzed on the RFoF links that had been installed for the AAVS2 system.

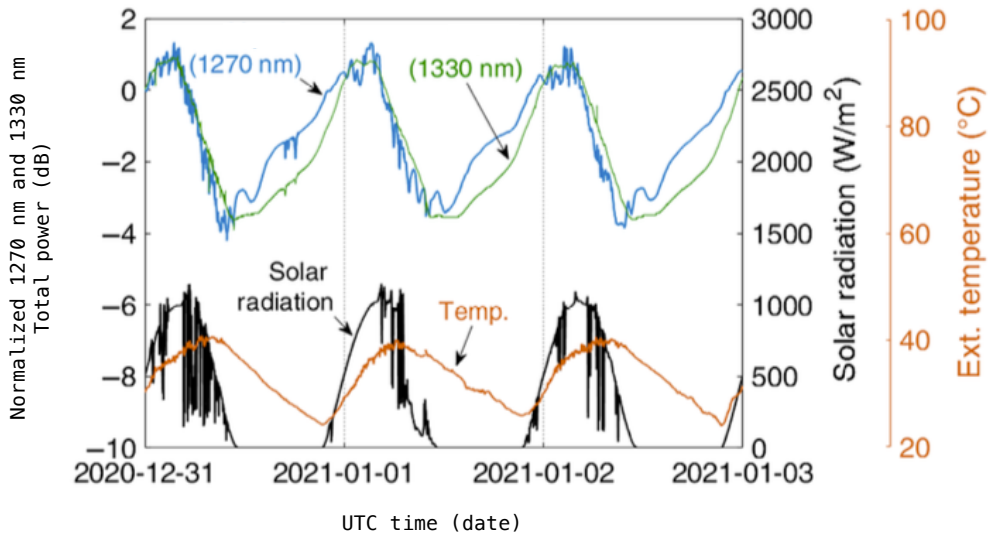

Figure 1.3 On the ordinate,1270 nm (λ_1) and 1330 nm (λ_2) power are reported. On bottom is possible to see the datetime at which the measurements refer. On right axes measurements of solar radiation and temperature taken from the Commonwealth Scientific and Industrial Research Organization (CSIRO) in order to correlate the behavior of the total RF power with climatic conditions.

The fluctuations are caused by polarization dependence of the optical receivers (EZconn BOSA) utilized in AVVS2.

The data presented in Figure 1.3 illustrates three days' worth of measurements that were taken on-site, capturing the total RF power at 160 MHz for both λ_1 and λ_2 components. These measurements were obtained from a single AAVS2 antenna and were transmitted to the PREADU via an RFoF link that was approximately 5.5 Km in length and laid out on the ground. The values of the RF power were normalized to their respective initial values.

The observed fluctuations were found to be related to external environmental factors, such as temperature, that were affecting the optical fiber cable used in the system.

The unexpected behavior, which was observed, was attributed to a combination of factors, specifically the polarization mode dispersion (PMD) of the optical fiber and the Polarization-Dependent Loss (PDL) of the WDM TFF (Thin Film Filter).

The PDL was due to the polarization-dependent reflection and transmission coefficients of the filter that was located at the receiver side.

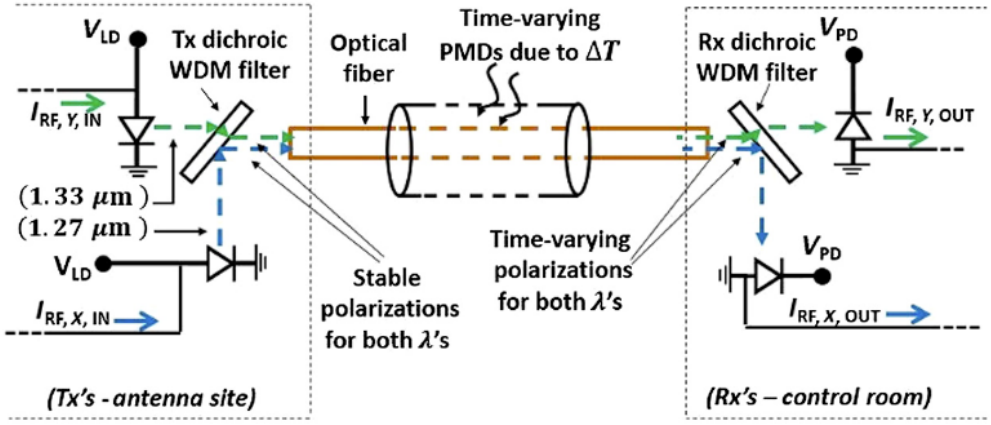

Figure 1.3.1 scheme which illustrates the mechanism causing the RF power fluctuations.

Due to the stable polarization of the optical signals coming from each of the two LASERs, any inherent difference in the reflection and transmission coefficients of TFF, based on whether the incident field has x or y polarization, does not cause any undesired fluctuations in the optical powers entering the optical fiber. Specifically, the optical field at 1330 nm (green dashed in Figure 1.3.1) that passes through the dichroic WDM filter located at the transmitter site will experience an equivalent transmission coefficient that is stable over time. Similarly, the equivalent reflection coefficient that is experienced by the optical field at 1270 nm (blue dashed in Figure 1.3.1) will also be stable over time.

The two optical fields (in this case, the one at 1330 nm and the one at 1270 nm) that hit the parallelepiped-like WDM TFF splitter, at the receiver side, have polarizations that change over time in contrast to the stable polarization of the optical signals at the transmitter side. This behavior results from changes in the environment over time along the fiber path, which in turn cause changes in the refractive index over time in various areas of the optical cable. These undesirable variations in the optical powers, which are picked up by the two photodiodes, are brought on by the polarization-dependent reflection and transmission coefficients of the dichroic filter.

1.4 Thesis organization

The goal of this thesis is to better understand and eventually reduce the impact of PMD/PDL on the RFoF SKA-low receiver.

In this first chapter, a general overview of the scenario on which the work was developed has been introduced.

Chapter 2 deals with the PDL of the optical receivers used in AAVS2 and then it proceeds with description about the measurement activity carried out on the PDL sensitivity of some BOSA and on the results obtained.

Chapter 3 is a theoretical introduction to the PMD problem and the statistical approach to treat it.

Chapters 4 and 5 present the simulation activity carried out with the relative results.

Chapter 2

Polarization Dependent Loss

The Polarization Dependent Loss (PDL) is the maximum peak-to-peak insertion loss (or gain) variation, which could be produced by optical component when stimulated by all possible polarization state. It is expressed in dB units.

$$PDL\ [dB]=P_{out,max} - P_{out,min} \qquad \textbf{(2)}$$

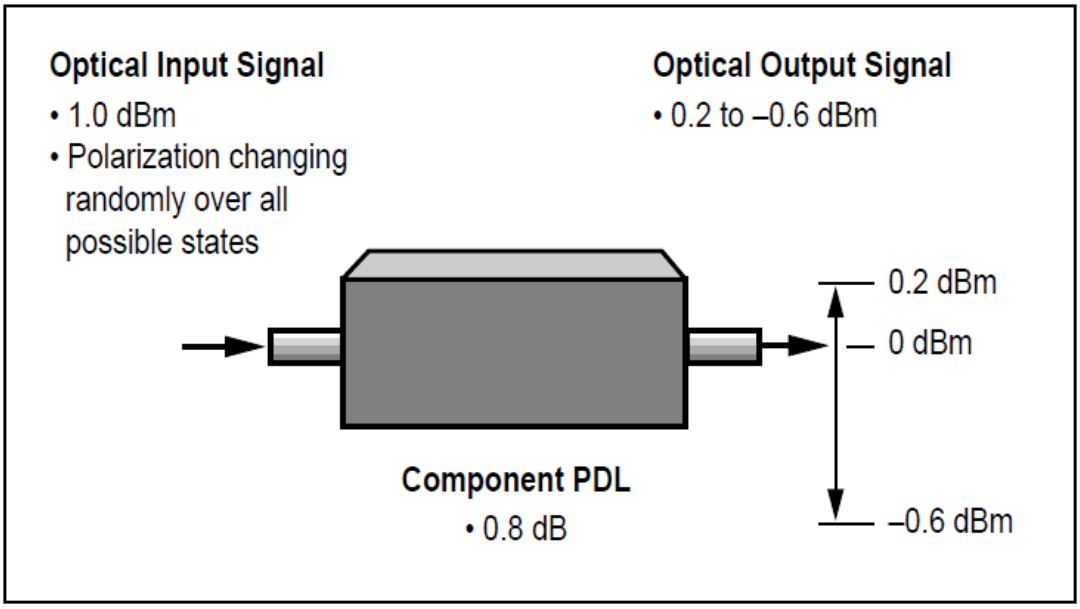

Figure 2. It reports an example where optical input signal has 1 dBm power and its polarization changing randomly over all possible states, which enters into PDL dependent optical components. At the output is possible to see how optical output signal's power fluctuates in a range of values that varies from -0.6 dBm to 0.2 dBm. This means that, by definition, the PDL is of 0.8 dBm.

Other names referred to PDL are, for example, polarization sensitivity or polarization gain.

2.1 AAVS2 WDM PDL description

The objective is to analyze the PDL because of the AAVS2 thin film filter's polarization-dependent transmission and reflection coefficients, as was already indicated in section 0.3. The last fiber span, with a certain rotation angle α_N, and the WDM TFF, that is attached to it, are thus the main points of attention.

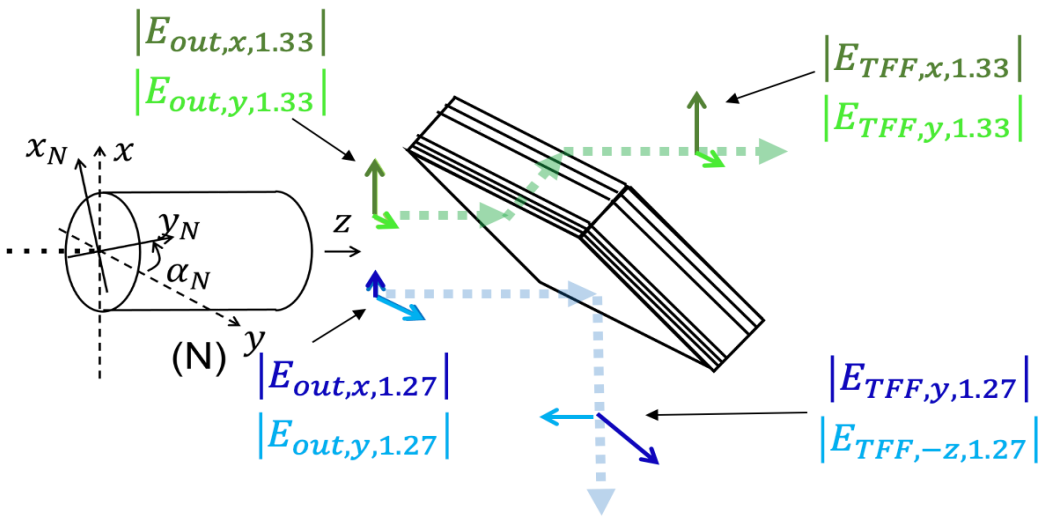

Figure 2.1 Last fiber span and WMD dichroic filter (TFF).

From Figure 2.1[4] is possible to see the TFF's behavior; in fact, in it is underlined how both the wavelengths are characterized by two polarized component (by two polarized components x and y, whose can be also called respectively TE and TM) and furthermore how $\bar{E}_{out,\lambda_{1=1.27}}$ and $\bar{E}_{out,\lambda_{2=1.33}}$ are respectively reflected and transmitted by the TFF.
To mathematically demonstrate the relationship introduced by the TFF, it is necessary to define two matrices:

(2.1.1)

$$W_{\lambda_1} = \begin{pmatrix} |S_{11,x=TE}|_{\lambda_1} & 0 \\ 0 & |S_{11,y=TM}|_{\lambda_1} \end{pmatrix}$$

$$W_{\lambda_2} = \begin{pmatrix} |S_{21,y=TM}|_{\lambda_2} & 0 \\ 0 & |S_{21,x=TE}|_{\lambda_2} \end{pmatrix} \qquad \textbf{(2.1.2)}$$

Where $S_{11,TE}$ and $S_{11,TM}$ are defined as the TE, TM TFF's reflection coefficients for λ_1 TE, TM components. In the same way $S_{21,TM}\ and\ S_{21,TE}$ are the TFF's transmission coefficients for λ_2.

Through the matrices definition is possible to describe the TFF reflected ($\bar{E}_{TFF,\lambda_1}$) and transmitted ($\bar{E}_{TFF,\lambda_2}$) fields:

$$\bar{E}_{TFF,\lambda_1} = W_{\lambda_1} \text{x } \bar{E}_{out,\lambda_1} \qquad \textbf{(2.1.3)}$$

$$\bar{E}_{TFF,\lambda_2} = W_{\lambda_2} \text{x } \bar{E}_{out,\lambda_2} \qquad \textbf{(2.1.4)}$$

Each field is composed by two polarized components, as known, hence, the following expressions are obtained:

$$\begin{pmatrix} |E_{TFF,y,\lambda_1}| \\ |E_{TFF,-z,\lambda_1}| \end{pmatrix} = \begin{pmatrix} |S_{11,TE}|_{\lambda_1,} & 0 \\ 0 & |S_{11,TM}|_{\lambda_1} \end{pmatrix} \begin{pmatrix} |E_{out,x,\lambda_1}| \\ |E_{out,y,\lambda_1}| \end{pmatrix} \qquad \textbf{(2.1.5)}$$

$$\begin{pmatrix} |E_{TFF,x,\lambda_2}| \\ |E_{TFF,y,,\lambda_2}| \end{pmatrix} = \begin{pmatrix} |S_{21,TE}|_{\lambda_2} & 0 \\ 0 & |S_{21,TM}|_{\lambda_2} \end{pmatrix} \begin{pmatrix} |E_{out,x,\lambda_2}| \\ |E_{out,y,\lambda_2}| \end{pmatrix} \qquad \textbf{(2.1.6)}$$

In the previous chapters, it has been discussed how AAVS2 prototype is exposed to the strong temperature ranges of the Australian desert, and how these have an impact on the

birefringent material and on the mode polarization. Furthermore, it has been discussed how TFF is sensitive to continuous polarization changes.
All this leads to the conclusion that, it is of fundamental importance to take into account the PDL and what is its impact on the optical power received by the PREADU (since PDL was defined as an attenuation).
It is possible to identify the transmitted and reflected optical power by the WDM TFF.
The total optical transmitted power will be the sum between transmitted power along x and y directions:

$$P_{out,\lambda_2} = P_{out,\lambda_2,x,min} + P_{out,\lambda_2,y,max} \quad \textbf{(2.1.7)}$$

By exploiting similar consideration, the total reflected power is obtained:

$$P_{out,\lambda_1} = P_{out,\lambda_1,y} + P_{out,\lambda_1,-z} \quad \textbf{(2.1.8)}$$

The optical power is proportional to the electric field's square magnitude, as demonstrated in subparagraph 1.1.5, it follows that the powers can be expressed as:

$$P_{out,\lambda_2} = |E_{TFF,x,\lambda_2}|^2 + |E_{TFF,y,\lambda_2}|^2 \quad \textbf{(2.1.9)}$$

$$P_{out,\lambda_1} = |E_{TFF,-z,\lambda_1}|^2 + |E_{TFF,y,\lambda_1}|^2 \quad \textbf{(2.1.10)}$$

To make the discussion more fluent, it is convenient to analyze the two equations and the related terms separately.
Let's consider P_{out,λ_2}'s terms:

$$P_{out,\lambda_2,x,min} = |E_{TFF,x,\lambda_2}|^2 = |s_{21,TE,\lambda_2}|^2 |E_{out,x,\lambda_2}|^2 \quad \textbf{(2.1.11)}$$

$$P_{out,\lambda_2,y,max} = |E_{TFF,y,\lambda_2}|^2 = |s_{21,TM,\lambda_2}|^2 |E_{out,y,\lambda_2}|^2 \quad \textbf{(2.1.12)}$$

The TE, TM transmission coefficients (for a TFF) are defined as:

$$|S_{21,TE,\lambda_2}|^2 = 10^{-\frac{PDL\_TFF\_dB\_TE\_\lambda_2}{20}} \quad \textbf{(2.1.13)}$$

$$|S_{21,TM,\lambda_2}|^2 = 1 \quad \textbf{(2.1.14)}$$

Where exponent $PDL\_TFF\_dB\_TE\_\lambda_2$ holds for the attenuation in dB introduced by the TFF's TE transmission coefficient on the $\lambda_2's$ power (in other words on the power transmitted by the TFF).
Similar considerations are done for P_{out,λ_1}:

$$P_{out,\lambda_1,-z,min} = |E_{TFF,-z,\lambda_1}|^2 = |S_{11,TM,\lambda_1}|^2 |E_{out,y,\lambda_1}|^2 \quad \textbf{(2.1.15)}$$

$$P_{out,\lambda_1,y,max} = |E_{TFF,y,\lambda_1}|^2 = |S_{11,TE,\lambda_1}|^2 |E_{out,x,\lambda_1}|^2 \quad \textbf{(2.1.16)}$$

Where TE, TM reflection coefficients are defined as follow:

$$|S_{11,TE,\lambda_1}|^2 = 1 \quad \textbf{(2.1.17)}$$

$$|S_{11,TM,\lambda_1}|^2 = 10^{-\frac{PDL\_TFF\_dB\_TM\_\lambda_1}{20}} \quad \textbf{(2.1.18)}$$

This time $PDL\_TFF\_dB\_TM\_\lambda_1$ holds for the attenuation in dB introduced by the TFF's TM reflection coefficient on the $\lambda_1's$ power (in other words on the power reflected by the TFF).
Through these passages, it is possible to define the PDL coefficients that characterized the TFF utilized in AAVS2 prototype. They hold respectively for λ_2 and λ_1.

$$\mathrm{PDL}_{\lambda_2=1.33} = 10\log_{10}\left(\frac{\left|\mathrm{S}_{21,\mathrm{TM},1.33}\right|^2}{\left|\mathrm{S}_{21,\mathrm{TE},1.33}\right|^2}\right) \quad \textbf{(2.1.19)}$$

$$\mathrm{PDL}_{\lambda_1=1.27} = 10\log_{10}\left(\frac{\left|\mathrm{S}_{11,\mathrm{TE},1.27}\right|^2}{\left|\mathrm{S}_{11,\mathrm{TM},1.27}\right|^2}\right) \qquad \textbf{(2.1.20)}$$

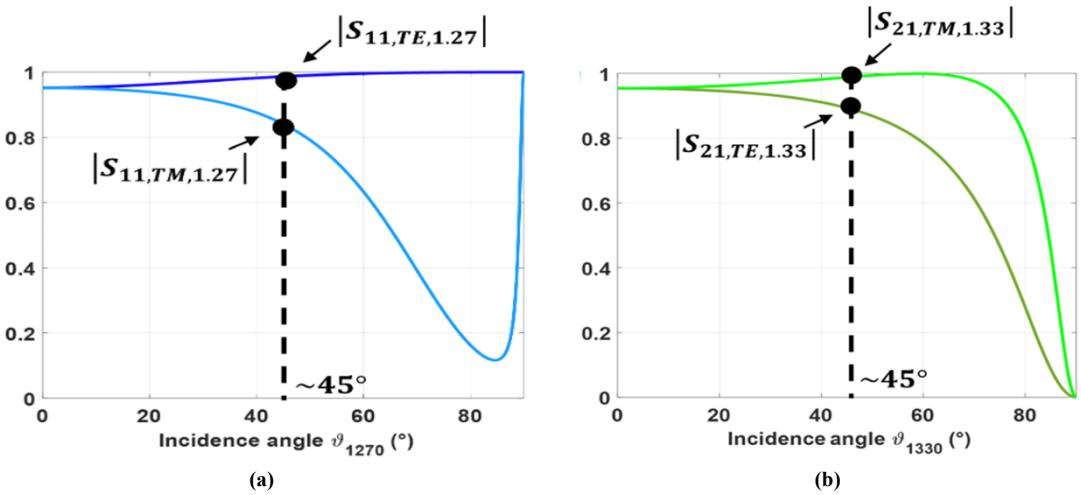

Figure 2.1.2 on the ordinate the are the attenuation values expressed in dB, while on the abscissa there are the TFF's incidence angles. In **(a)** are reported the reflection coefficients for the λ_1 polarized signal, in **(b)** the transmission coefficients for λ_2 polarization.

Figure 2.1.2 aims to provide concrete example on the framework discussed so far; at this purpose, it reports two graphs, where a TFF inclined with an angle of 45° is considered equivalent to AAVS2 case.

From (a) and (b) is possible to derive PDL coefficients from both λ_1 and λ_2 polarized incident signals.

According to (2.1.19) and (2.1.20):

$$\mathrm{PDL}_{\lambda_2}[dB] = 0.1 \qquad \textbf{(2.1.20)}$$

$$\mathrm{PDL}_{\lambda_1}[dB] = 0.2 \qquad \textbf{(2.1.21)}$$

Pertaining with the example's results ((2.1.20 and 2.1.21)), P_{out,λ_1} and P_{out,λ_2} can have respectively fluctuations of 0.2 and 0.1 dB around their values, because of TFF's PDL_{λ_1} and PDL_{λ_2} coefficients.

2.2 PDL evaluation on SSopt BOSA PD

A laboratory test was performed on RFoF system to quantify the PDL impact depending on the WDM BOSA, which are implementend on 14 PREADU.

Those optical receivers are produced by the SSopt (chineese facility).

This test provides only measurements on PDL, the PMD is neglected.

Each PREADU contains 8 BOSA (WDM ORX) and for each was evaluated the PDL impact on the total RF received power.

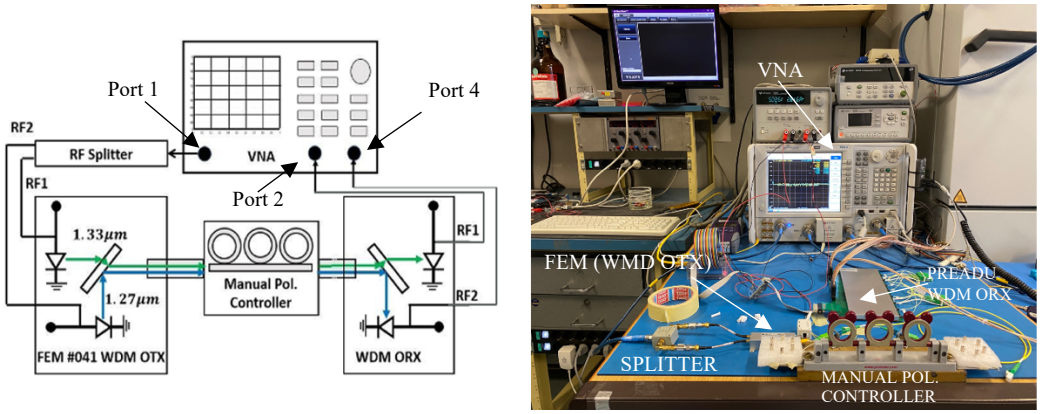

Figure 2.2 Experimental setup utilized to determine to measure the PDL of the SSopt WDM BOSA PD, that will be implemented in the AAVS3 PREADU. On left the block scheme setup is reported, while on right there is the real laboratory setup.
In the block scheme, for simplicity, there is only the WDM ORX BOSA and not the complete PREADU architecture. This choice was made to emphasize this kind of WDM ORX is the optical receiver presently utilized in RFoF system.

Port 1 Power Level = -60 dBm
Continuos wave frequency =192 MHz
Time sweep = 50 sec

Table 2.2

The VNA utilized is the PNAx, which provides high measurement accuracy, an extended frequency range, and greater flexibility in measurement configuration compared to other traditional VNAs.

As illustrates by Table 2.2, for PNAx calibration, 192 MHz was chosen as continuous wave frequency (which means that there is only one frequency tone), -60 dBm as power level to generate RF signal from Port 1 and time sweep of 50 seconds within which 1001 data acquisition points were set.

The splitter splits the original RF signal, in RF_1 and RF_2; within FEM, WDM OTX laser sources modulate RF_1 and RF_2 respectively at λ_2 and λ_1. Immediately afterwards the two modulated signals are multiplexed to be simultaneous transmitted through the same fiber.

The Manual Polarization Controller (also called Mickey Mouse) was used to reproduce the polarization variations, that depend on temperature variations at the MRO site.

WDM ORX separates the λ_2 and λ_1 signals and demodulates them.

WDM ORX has RF_1 and RF_2, in fact it will transmit the RF_1 component and it will reflect the RF_2 one.

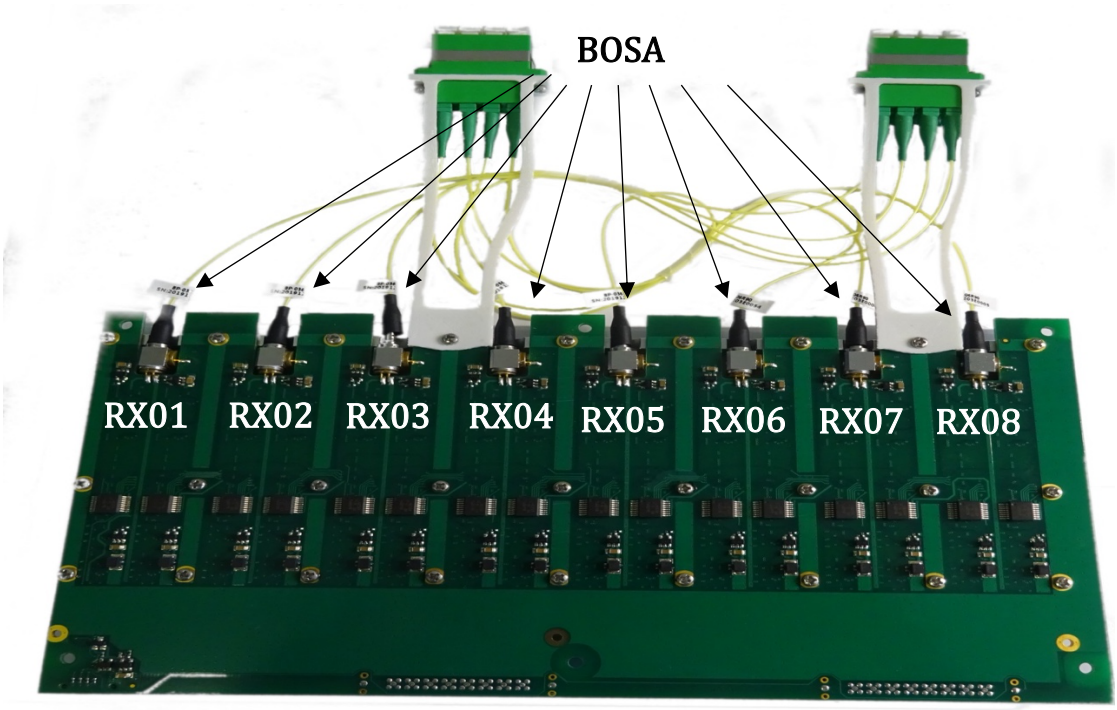

Figure 2.2.1 AAVS3 PREADU is reported, where the BOSA are clearly underlined; each BOSA is numerated with RX nomenclature.

At the end, RF_1 and RF_2 enter in PNAx port 2 and 4. Both powers data are collected into a csv files. The PDL measurement is taken after csv files elaboration, through the use of other software (e.g. MATALAB, Excel).

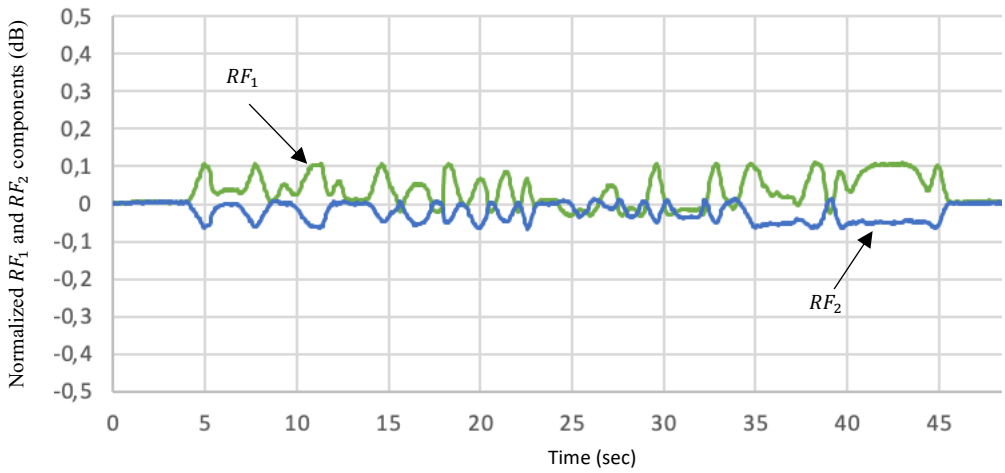

Figure 2.2.2

Figure 2.2.1 is an example of PDL measurements for both RF_1 and RF_2, due to the WDM ORX (BOSA 7) polarization dependence within SSopt R012 PREADU. Furthermore, is possible to appreciate how the RF_1 component (green curve) and RF_2 component (blue curve) show the same time evolution, indeed their behaviors are correlated and opposite.

2.3 Statistical analysis on PDL measurements for Ssopt BOSA

A statistical analysis was offered to more accurately assess the information gathered from the PDL measurements.

The goal was achieved using a tool called boxplot and a MATLAB script was created for the purpose.

2.3.1 Boxplot introduction

To better understand the results that will be proposed, it is necessary to make a brief introduction to the boxplot.

A boxplot, also known as a box-and-whisker plot, is a graphical representation of a dataset showing its distribution and central tendency.

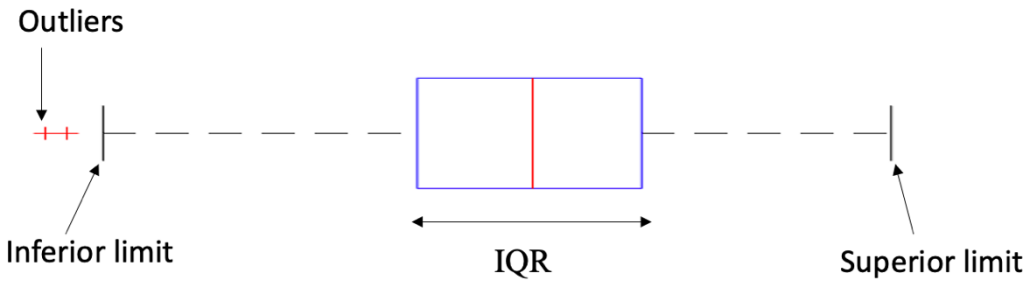

Figure 2.3 Typical graphical representation of boxplot

The blue box, in Figure 2.3, represents the interquartile range (IQR), which is the range between the 25th and 75th percentiles of the data (also called first quartile Q_1 and third quartile Q_3), in other words the 50% of the data are within the box. The median, or the middle value of the dataset, is represented by a horizontal red line inside the box. The whiskers extend from the box to the minimum and maximum values of the data that are not considered outliers and for this reason are called inferior and superior limits.
The mathematics, behind the whiskers, leads on the following expression:

$$\text{Inferior limit} = Q_1 - 1.5*\text{IQR} \quad \textbf{(2.3.1)}$$

$$\text{Superior limit} = Q_3 + 1.5*\text{IQR} \quad \textbf{(2.3.2)}$$

The outliers are identified by red crosses, and they hold for those data that are abnormal; due to their anomaly, they could disturb the whole statistic, that's why they are out of the whiskers.

2.3.2 MATLAB script description

All the data about the PDL measured on the 14 PREADU are collected onto 7 Excel files. Each file contains the data about two PREADU and theiery respectiveve 8 BOSA.
For each file there is a final sheet called “Recap” that gives the global view on the PDL values and the resulting mean value of the RF_1 and RF_2 output powers by each BOSA of each PREADU.

PDL	RX01	RX02	RX03	RX04	RX05	RX06	RX07	RX08	RX09	RX10	RX11	RX12	RX13	RX14	RX15	RX16
RF1	0,11	0,11	0,12	0,15	0,11	0,09	0,09	0,11	0,17	0,12	0,14	0,14	0,17	0,24	0,13	0,15
RF2	0,04	0,04	0,06	0,03	0,05	0,06	0,05	0,06	0,31	0,02	0,08	0,02	0,03	0,11	0,06	0,07
P_RF1 (dBm)	-4,42	-4,42	-5,03	-4,56	-4,45	-4,96	-5,40	-4,87	-4,45	-4,09	-4,83	-3,83	-4,94	-4,44	-3,79	-5,09
P_RF2 (dBm)	-5,75	-5,75	-5,36	-5,96	-5,88	-5,83	-6,47	-5,75	-6,14	-5,94	-6,66	-5,94	-6,25	-6,45	-6,09	-7,28

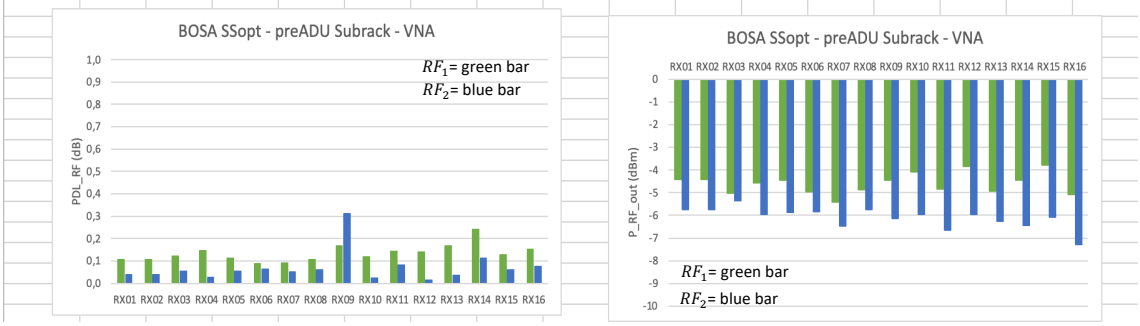

Figure 2.3.2.1 Example of recap sheet for R011-R012 PREADU. In first row, the columns that goes from RX01 to RX08 and from RX09 to RX16 identify, respectively the R011’s BOSA and the R012’s BOSA. In second and third rows, the optical receivers (BOSA) PDL values for RF_1 and RF_2 components. RX01, for example, identify one BOSA of the PREADU. In fourth and fifth rows are reported the mean powers values, of RF_1 and RF_2 powers. The mean was taken on all 1001 power values acquired, for both, in 50 seconds of time sweep.

The graph, on the Figure 2.3.2.1 left side, shows the PDL of the optical receivers that impacts on RF_1 and RF_2 polarizations. As is possible to notice, statistically, PDL values, for the RF_1 polarized receiver, are larger than the RF_2 ones. This is not always true but depends on BOSA manufacturer and, in particular, from the TFF adopted.

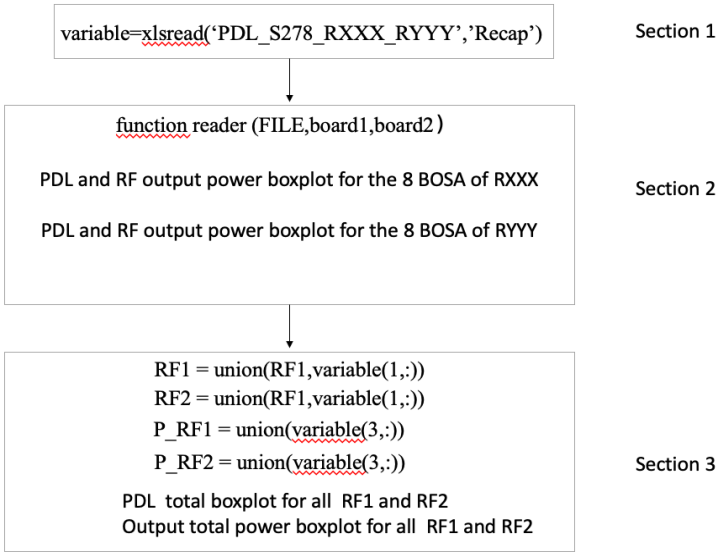

Figure 2.3.2.2 Code block scheme

The code provided is divided in three main sections, as reported in Figure 2.3.2.2.

In Section 1, the data are taken from the "Recap" sheet of seven Excel files named "PDL_S278_RXXX_RYYY,'Recap'", where "XXX" and "YYY" are the PREADU numbers, using the "xlsread" MATLAB function and then they are stored in variables.

In Section 2 is defined the function "reader". This is used to plot the boxplots of PDL and total RF output power for each PREADU.

The function takes the variables defined in Section 1 (one by one) as an input and plots two subplots with two boxplots each (one for the RF_1 and the other for RF_2).

The two boxplots aim to represent the statistics for both PDL values of optical receivers and of the mean values of output RF output power observed in each BOSA.

Actually, the mean RF output power values is irrelevant for PDL assestment; it is used to understand if a certain optical receiver works correctly, in other words if its mean output power value is in the expected range.

The PNAx generates a -60 dBm RF signal, the RF splitter introduces 3dB of attenuation, therefore about -63 dBm of power enter the FEM.

Since the optical receiver has a gain of 60 dBm, the expected mean received power value should be around -3 dBm (actually you receive a slightly lower value, e.g -5 dBm, due to the Mickey Mouse insertion loss).

Furthermore, in this section, the statistics of each single PREADU are derived separately

(the first 8 BOSA for RXXX and the second 8 BOSA for RYYY).

Since the primary scope is to have a global view on all SSopt's PDL sensitivity, in Section 3, the data, collected from all the 112 BOSA of the 14 PREADU, is merged to plot the final boxplots of the total PDL values and total mean RF output power values for RF_1 and RF_2.

2.3.3 Discussion on the results obtained

At the end of the code execution fifteen plots are printed on the screen.

Each of the first fourteen represents the total statistic on the PDL value and on the total output power of RF1 and RF2 of each single PREADU.

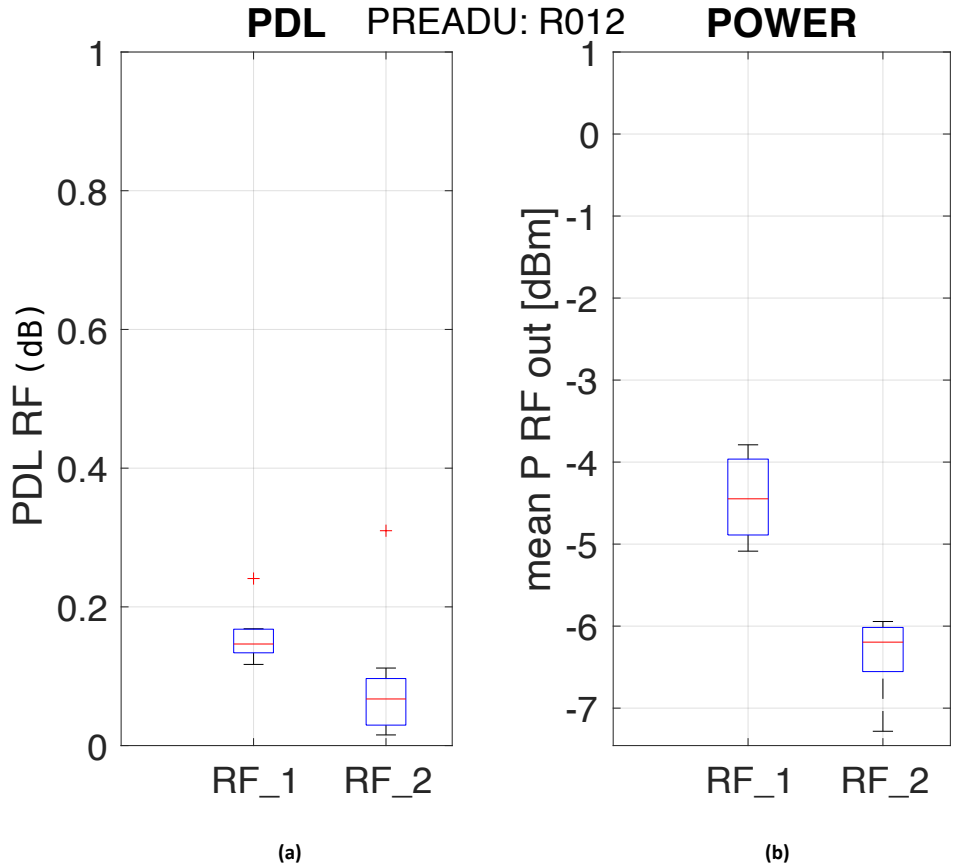

Figure 2.3.3.1 These are the boxplots for SSopt R012. **(a)** illustrates on the abscissa the RF_1 and RF_2 and on the ordinate the RF_PDL values in dB, for **(b)** holds the same concept, but on the ordinate, there are the mean output RF power values in dBm. For each subplot there is one boxplot for RF_1 and one for RF_2.

In **(a)**, PDL of optical receiver, for RF_1 is higher than the one for RF_2 (same conclusions deducted from Figure 2.3.2.1); indeed, PDL for RF_1 takes a value from 0.11 dB and 0.16

dB. Since superior limit and Q3 coincide, the 50% of data take a values between [0.13; 0.16] and the median at 0.14, while PDL for RF_2 goes from 0.01 to 0.11 with 50% of values between [0.02:0.9] (very small values) and the median at 0.06. Instead PDL RF_1's outlier, at 0.24, is smaller respect the PDL RF_2's one (at 0.13).

It is important to further reiterate that, these conclusions are valid for this particular case, but are not general because the PDL sensitivity of optical receiver depends on the type of TFF used, but also on the BOSA manufacture.

In **(b)**, the statistics on mean RF output power, for both RF_1 and RF_2 polarizations, is provided. The 100% (since no outliers are present) mean RF output power values for RF_1 are in the range between from [-5.08; -3.17] with the median at -4.44. The 50% values belong to the interval [-4.88; -3.96]. Also the boxplot for RF_2 does not present any outlier, hence the 100% of mean power output values are in the interval [-7.28;-5.94] with the median at -6.19. The 50% of values take a values in the range [-6.55;-6.01].

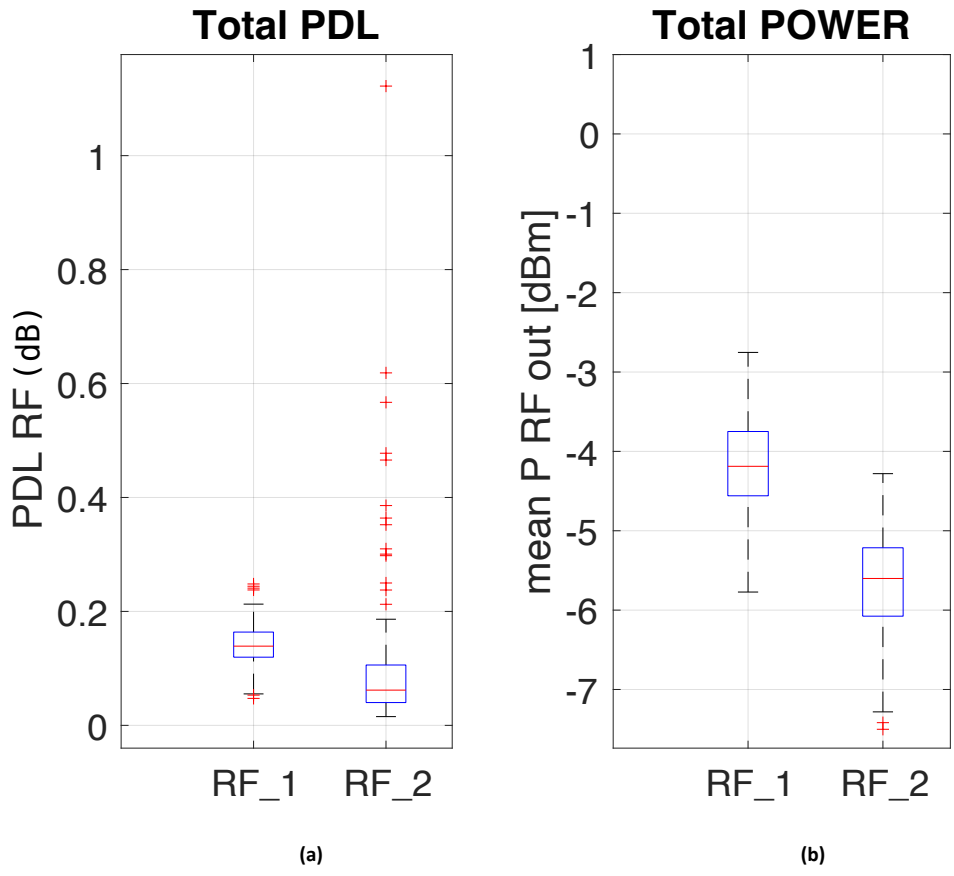

Figure 2.3.3.2

In Figure 2.3.3.2 illustrates the fifteenth plot, which aims to report the total statistics both on PDL values for the λ_2 and λ_1 polarized optical receivers implemented within all 112 BOSA of all PREADU and on the mean output power values for RF_1 and RF_2 components.

Figure (a) allows to have an important conclusion for the PDL point of view on the Ssopt. In fact, statistically, the optical receivers show a larger impact in terms of PDL values for the RF_1 respect to the RF_2 ones.

Going deeper in detail, it is possible to see how the last 75% PDL RF_1 takes values in range [0.11;0.21], that in general are not very low values; only first 25% of values are in between [0.02;0.11]. The median value is 0.13.

On the contrary, the first 75% PDL RF_2 takes values in range [0.01;0.1] and the last 25% of values are in between [0.1;0.18]. The median value is 0.06.

From outliers' point of view, things are different. In fact, the PDL outliers, for RF_2 component, are larger both in numbers and in values respect to the RF_1 case.

With (b) is possible to derive that, statistically, the mean RF_1 output power takes the 100% of values between a minimum of -5.77 and maximum of -2.75, since the outliers absence. Instead, the mean RF_2 output power show inferior limit of -7.282 and superior limit of -4.28. It shows two outliers below the inferior limit.

Moreover, with focus on the blue boxes of both is possible to assert that, on average, mean RF_1 output power is larger than the RF_2 one.

Chapter 3

Polarized Mode Dispersion

As the bit rate and distance of optical fiber transmission systems continue to increase, the understanding of polarization-mode dispersion (PMD) and its system impairments and mitigation are becoming ever more important.

Actual, fibers exhibit some birefringence as a result of impairments in the production process and mechanical stress after manufacture (or at least one of the two).

Optical birefringence and unpredictable variation in the orientation of the birefringent axes along the fiber length are the causes of PMD.

Different polarizations of PMD result in different delays, and when the difference between the delays gets close to a significant portion of the bit period, pulse distortion and system penalties happen.

The fiber PMD varies stochastically over time because of environmental changes, such as temperature and stress, making PMD particularly challenging to manage.

The RF signals received from the antenna are carried down by two separate currents, each of which carries a Y-polarized and X-polarized signal. These signals are then used to modulate lasers that emit at wavelengths of 1330 and 1270 nm, respectively.

The resulting optical signals are combined using a parallelepiped shaped WDM combiner with an incident angle of about 45 degrees relative to the vectors perpendicular to the respective incidence surfaces.

At the site where the optical transmitters are located, fluctuations in temperature can cause changes in the conversion efficiency of the lasers or the precise wavelength of the emitted fields. However, the polarization of the optical signals coming from each of the two lasers (TE, TM, or a combination of both) is relatively stable over WDM combiner with an incident angle of about 45 degrees relative to the vectors perpendicular to the respective incidence surfaces.

For SKAlow receiver G652D fibers are chosen; hence the optical cable contains 256 G652D fibers that go from the log-periodic antennas to the data processing facilities.

The cable is made by loose structure, this architecture would not cause the fibers to experience an extra PMD difference because the fibers would already be under minimal

or even no stress from the cable structure. Hence, among all enclosed fibers, typical loose cable should have a lower and more consistent PMD.

3.1.1 Short discussion on light polarization

A lightwave's electric and magnetic fields oscillate perpendicular to the direction of propagation (z), at right angles to one another. The electric field, which interacts more strongly with most devices, is used to define polarization.

An elliptical point charge moving in the source's plane can be used to represent the electric field of a fully polarized, monochromatic light wave (Figure 1.1).

The major to minor axis ratio, angular orientation, and direction of rotation of the ellipse, all provide information about the polarization of the light. Extreme examples of elliptical polarization include linear and circular polarizations.

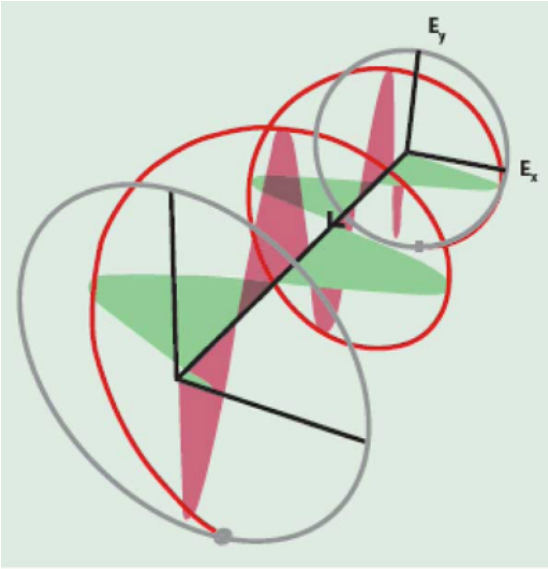

Figure 3.1 from https://www.photonics.com/Articles/Polarization_Mode_Dispersion_Concepts

The Poincaré sphere offers an illustrative shorthand for polarization states. A distinct state of polarization is represented by each point on the sphere's surface. At the poles are circular states and at the equator are linear ones. The northern and southern hemispheres, respectively, are home to the right-handed and left-handed elliptical states.

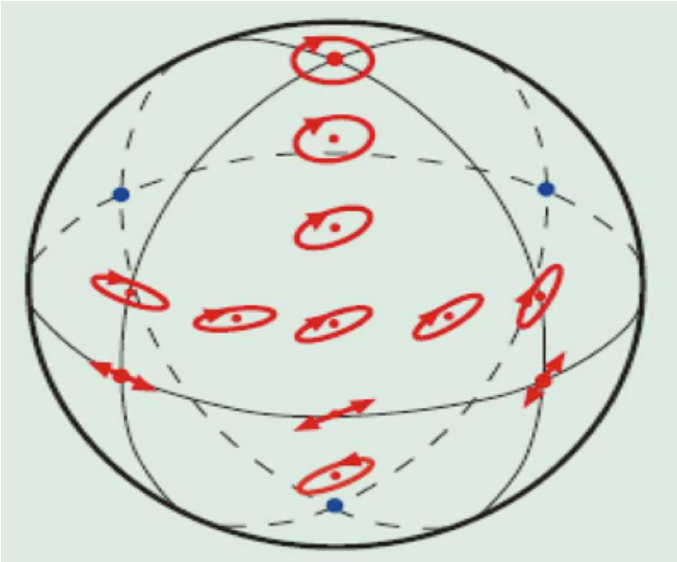

Figure 3.1.2 A different polarization state is represented by each point on the Poincaré sphere.

The concept of orthogonality refers to the mathematical independence of polarization states that are diametrically opposed to one another. Examples of orthogonal states include linear horizontal and vertical polarizations, where light coming from one is blocked by the other[5].

3.1.2 Causes of Birefringence and consequences

In optics PMD is the third type of dispersion (after multimodal dispersion and chromatic dispersion); it is very similar to the multimodal one, but to observe it, it is advisable to consider single mode fiber (LP_{01}).

Even if telecommunications fibers are often called single mode (LP_{01}), there are two orthogonally polarized modes.

The linear superposition of two LP_{01} modes with orthogonal polarizations ($LP_{01,x}$ and $LP_{01,y}$) can be used to represent an electromagnetic field with arbitrary polarization in a single-mode optical fiber.

For the moment, as a reference is taken an ideal case, that is the perfect circularity of fiber's waveguide.

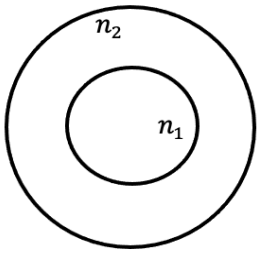

Figure 3.1.2.1: ***perfect circular fiber where n_1 and n_2 are respectively the core and cladding refraction indices. With $n_2 > n_1$***

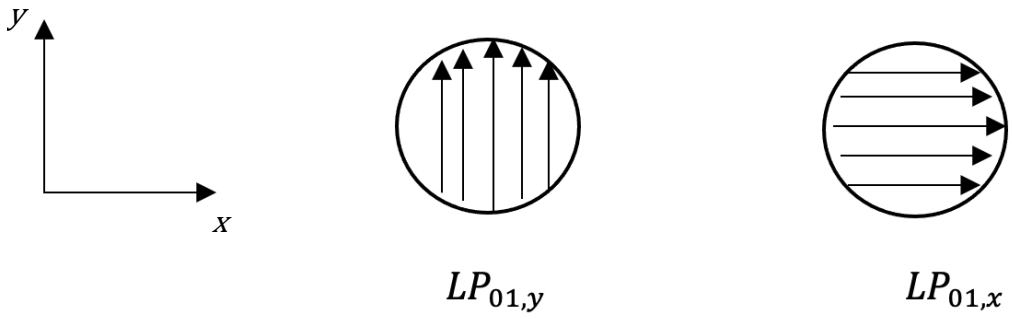

Figure 3.1.2.2 (From left to right): orthogonal reference system and orthogonal polarized modes.

Under this condition, thanks to transverse plane's circular symmetry of the waveguide, the two modes $LP_{01,x}$ and $LP_{01,y}$ are indistinguishable, in formal words they are called degeneracy and this leads to $\beta_{LP_{01,x}} = \beta_{LP_{01,y}}$, which means that the constants of phase, that refer respectively to $LP_{01,x}$ and $LP_{01,y}$, are the same.

Since the group delay is defined as $\tau_g = \frac{d\beta}{d\omega}$, another consequence of degenerate modes is that the group delays, of the two modes, τ_{g_x} and τ_{g_y} are the same.

The group velocity is defined as $v_g = \frac{1}{\tau_g}$, and also for this notion holds the same concept as before.

Unfortunately, because of imperfections in the manufacturing process and/or mechanical stress after fabrication, fibers lost circular symmetry and become somehow asymmetrical. The orthogonally LP_{01} polarized modes degeneracy is broken by the asymmetry, leading to birefringence, that is a difference in the phase and group delays of the two modes.

Birefringence is due to intrinsic phenomenon, if it is caused by the manufacturing imperfections, but it arises from extrinsic point view, when a non circular waveguide is considered.

Figure 3.1.2.3 ***(From left to right): orthogonal reference system and orthogonal polarized modes.***

Birefringence can be produced by a variety of extrinsic perturbations, including lateral stress, bending, or twisting, when fiber is spooled, cabled, or embedded in the ground. As the fiber's surrounding environment changes, these perturbations will as well.

In a single mode fiber, as already discussed, the electromagnetic field with an arbitrary polarization can be expressed by the linear superposition of two modes $LP_{01,x}$ and $LP_{01,y}$ with orthogonal polarizations.

The generic field $\vec{E}$, that propagates through the fiber, can be expressed as:

$$\vec{E} = E_x\,\hat{x} + E_y\hat{y} \qquad \textbf{(3.1.2.1)}$$

E_x , E_y are the field's polarized components along the direction ($\hat{x}$, $\hat{y}$) and they are referred respectively to $LP_{01,x}$ and $LP_{01,y}$.

If subjected to an external perturbation, a single mode fiber becomes "bimodal", due to the loss of the degeneracy condition of the LP_{01} modes. In this case, the fiber can be

considered as a birefringent linear medium, with different effective refractive indices $n_{eff,x}$ and $n_{eff,y}$ along the two principal birefringence axes.

3.1.3 Propagation through fiber with ideal circular waveguide

Let's consider a short section of fiber with ideal circular waveguide.
For sake of simplicity, let's impose that the polarized component of the field along x is 0, so that:

$$\vec{E} = E_y \hat{y} \qquad \textbf{(3.1.3.1)}$$

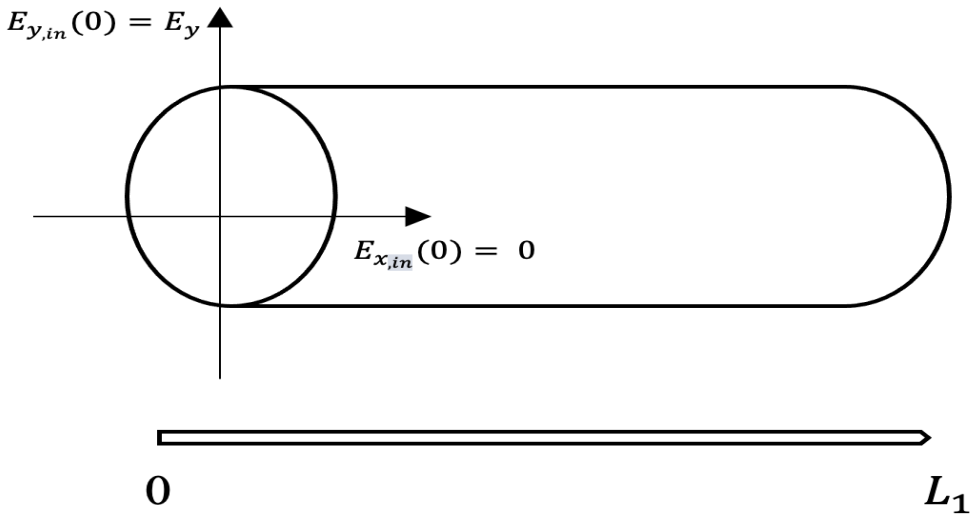

Figure 3.1.3.1: short fiber section of length L_1 and the input field's polarized components

In order to describe the transformation of the polarization state vector of the electromagnetic wave along a section of a circular waveguide fiber of length L_1, the Jones matrix $T(L_1)$ is introduced.
In general terms it is defined as a 2x2 complex matrix equal to:

$$T(L) = \begin{pmatrix} e^{-jn_{eff,x}k_0 L} & 0 \\ 0 & e^{-jn_{eff,y}k_0 L} \end{pmatrix} \quad \textbf{(3.1.3.2)}$$

Now it's possible to define which is the polarization of $\vec{E}_{out}(L_1)$:

$$\vec{E}_{out}(L_1) = E_{x,out}(L_1)\hat{x} + E_{y,out}(L_1)\,\hat{y} \quad \textbf{(3.1.3.3)}$$

$$\begin{pmatrix} E_{x,out}(L_1) \\ E_{y,out}(L_1) \end{pmatrix} = \begin{pmatrix} e^{-jn_{eff,x}k_0 L_1} & 0 \\ 0 & e^{-jn_{eff,y}k_0 L_1} \end{pmatrix} \begin{pmatrix} E_{x,in}(0) \\ E_{y,in}(0) \end{pmatrix} \quad \textbf{(3.1.3.4)}$$

$$\vec{E}_{out}(L_1) = E_{x,in}(0)\, e^{-jn_{eff,x}k_0 L_1}\hat{x} + E_{y,in}(0)\, e^{-jn_{eff,y}k_0 L_1}\hat{y} \quad \textbf{(3.1.3.5)}$$

With $E_{x,out}(L_1) = E_{x,in}(0)\, e^{-jn_{eff,x}k_0 L_1}$ and $E_{y,out}(L_1) = E_{y,in}(0)\, e^{-jn_{eff,y}k_0 L_1}$.
Since $E_{x,in}(0)$ is 0 and $E_{y,in}(0)$ is E_y, the output field is:

$$\vec{E}_{out}(L_1) = E_y e^{-jn_{eff,y}k_0 L_1}\hat{y} \quad \textbf{(3.1.3.6)}$$

The result is the one expected since circular symmetry was imposed, so the degeneracy property of the mode is satisfied.

3.1.4 Propagation through fiber with non-ideal circular waveguide

Let's consider the same section of the fiber and suppose an extrinsic perturbation that modify its circular waveguide. In this situation, the previous discussion must be modified, because the geometry of the medium follows a different shape and therefore the result will be different.

In fact, this time the field's components are polarized coherently with the new birefringence axes (x_1, y_1).

In the following figure is possible to see how the birefringence axis exhibit a rotation displacement of an angle α_1 respect to the axes considered so far.

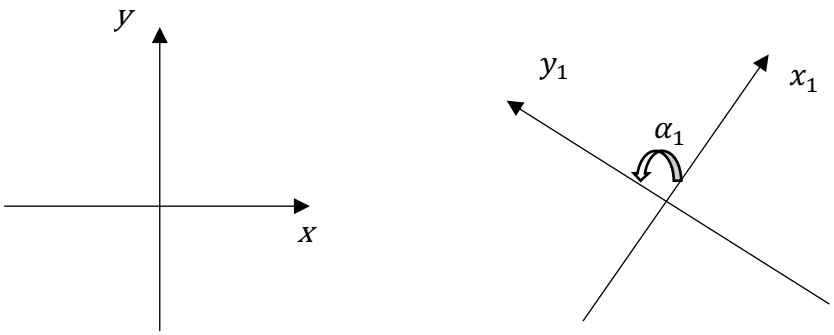

Figure 3.1.4.1

Even in this case, $\vec{E}$ is a generic field, which before entering the fiber segment, is equal to the sum of $\vec{E}_x$ and $\vec{E}_y$ (for simplicity $\vec{E}_x$ is 0). As before they are referred respectively to $LP_{01,x}$ and $LP_{01,y}$.

$$\vec{E} = E_y \hat{y} \qquad \textbf{(3.1.4.1)}$$

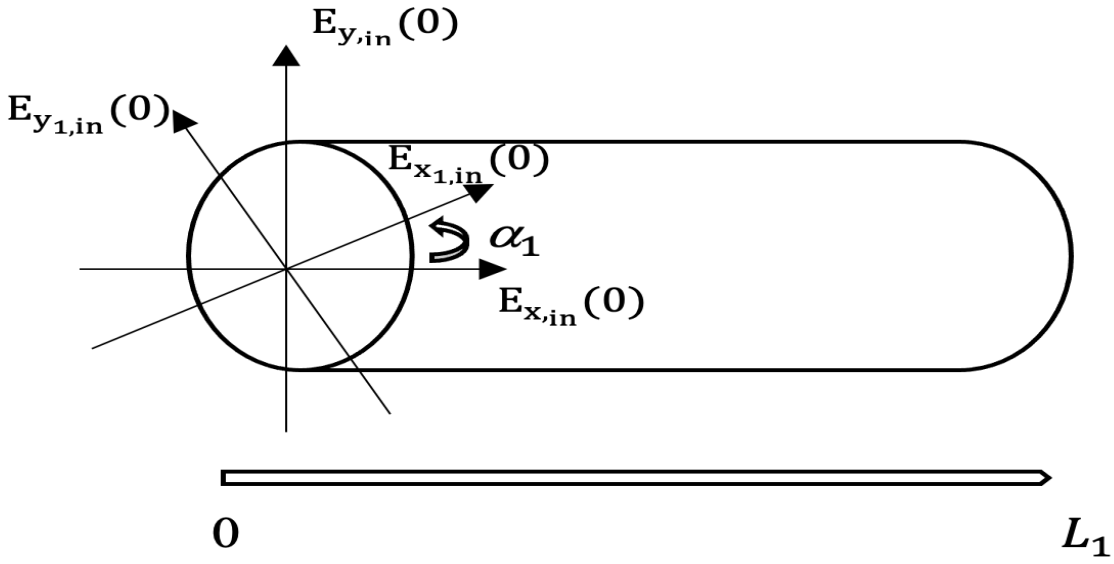

Figure 3.1.4.2

In Fig. 5, $\vec{E}$ is placed at the input of section and it is composed by the sum of the components $E_{x_{1,in}}\hat{x}$ and $E_{y_{1,in}}\hat{y}$.

Referring to the figure, the two components are polarized according to the birefringence axes (x_1, y_1); because of this, now they are referred to LP_{01,x_1} and LP_{01,y_1} .

Since, now, the fiber is a birefringent medium, it is necessary to take in account two different refractive indices $n_{eff,x_1}$and n_{eff,y_1} along the new birefringent axes (x_1, y_1).

The mathematical description of the concept is given by the following passages:

$$\vec{E}_{\ in}(0) = E_{x_{1,in}}(0)\hat{x}_1 + E_{y_{1,in}}(0)\,\hat{y}_1 \qquad \textbf{(3.1.4.2)}$$

In order to define the two field components, the rotation matrix R (2x2) has to be defined:

$$R = \begin{pmatrix} cos\alpha_1 & sin\alpha_1 \\ -sin\alpha_1 & cos\alpha_1 \end{pmatrix} \quad \textbf{(3.1.4.3)}$$

So that:

$$\vec{E}_{in,1} = R \times \vec{E}_{in} \quad \textbf{(3.1.4.4)}$$

$$\begin{pmatrix} E_{x_{1,in}}(0) \\ E_{y_{1,in}}(0) \end{pmatrix} = \begin{pmatrix} cos\alpha_1 & sin\alpha_1 \\ -sin\alpha_1 & cos\alpha_1 \end{pmatrix} \begin{pmatrix} E_{x,in}(0) \\ E_{y,in}(0) \end{pmatrix} \quad \textbf{(3.1.4.5)}$$

Where $E_{x,in}(0) = E_x = 0$ and $E_{y,in}(0) = E_y$.

The matrix calculation leads to:

- $E_{x_{1,in}}(0) = E_y \, sin\alpha_1$ **(3.1.4.6)**
- $E_{y_{1,in}}(0) = E_y \, cos\alpha_1$ **(3.1.4.7)**

It can be seen how the rotation of the reference system has caused the appearance $E_{x_{1,in}}(0)$ component, which according with the ideal case, was null.

In the same way let's consider the propagation through the section, dealing with the Jones matrix T(L).

$$\vec{E}_{out,1} = \mathrm{T}(\mathrm{L}_1) \text{ x } \vec{E}_{in,1} \qquad \textbf{(3.1.4.8)}$$

$$\begin{pmatrix} E_{x_1,out}(\mathrm{L}_1) \\ E_{y_1,out}(\mathrm{L}_1) \end{pmatrix} = \begin{pmatrix} e^{-jn_{eff,x_1}k_0\mathrm{L}_1} & 0 \\ 0 & e^{-jn_{eff,y_1}k_0\mathrm{L}_1} \end{pmatrix} \begin{pmatrix} E_{x_1,in}(0) \\ E_{y_1,in}(0) \end{pmatrix} \qquad \textbf{(3.1.4.9)}$$

$$\vec{E}_{out}(\mathrm{L}_1) = E_{x_1,out}(\mathrm{L}_1)\,\hat{x}_1 + E_{y_1,out}(\mathrm{L}_1)\,\hat{y}_1 \qquad \textbf{(3.1.4.10)}$$

With $E_{x_1,out}(\mathrm{L}_1) = E_{x_1,in}(0)\, e^{-jn_{eff,x_1}k_0\mathrm{L}_1}$ and $E_{y_1,out}(\mathrm{L}_1) = E_{y_1,in}(0)\, e^{-jn_{eff,y_1}k_0\mathrm{L}_1}$.
By substituting the equations of $E_{x_1,in}(0)$ and $E_{y_1,in}(0)$ to $\vec{E}_{out}(\mathrm{L}_1)$'s formula:

$$\vec{E}_{out}(\mathrm{L}_1) = E_y\, sin\alpha_1 e^{-jn_{eff,x_1}k_0\mathrm{L}_1}\hat{x}_1 + E_y\, cos\alpha_1 e^{-jn_{eff,y_1}k_0\mathrm{L}_1}\hat{y}_1 \qquad \textbf{(3.1.4.11)}$$

From $\vec{E}_{out}(\mathrm{L}_1)$ is possible to see how one part of E_y is polarized along x_1 and another along y_1.
The two refractive indices $n_{eff,x_1} and\ n_{eff,y_1}$ in a birefringent medium are different, so also the phase constants $\beta_{LP_{01,x}}$, $\beta_{LP_{01,y}}$ are different.

In a short section the birefringence can be considered uniform, and it can be modelled by considering the difference between the two phase constants that refer to the orthogonal polarized modes $LP_{01,x}$ and $LP_{01,y}$.
The birefringence coefficient is defined as:

$$\Delta\beta = \beta_{LP_{01,x_1}} - \beta_{LP_{01,y_1}} = (n_{eff,x_1} - n_{eff,y_1})k_0 = \Delta n_{eff}\frac{2\pi}{\lambda} \quad \textbf{(3.1.4.12)}$$

Since $\lambda = \frac{2\pi c}{\omega}$ the previous equation becomes:

$$\Delta\beta = \Delta n_{eff}\frac{c}{\omega} \quad \textbf{(3.1.4.13)}$$

Where Δn_{eff} is the differential effective refractive index, c is the speed of light and ω is the angular frequency. Typical values of Δn_{eff} span within a range of $[10^{-7} - 10^{-5}]$.
Under this definition the Jones matrix can be treated:

$$\mathrm{T}(\mathrm{L}_1) = e^{j\frac{(n_{eff,x_1}+n_{eff,y_1})k_0\mathrm{L}_1 t}{2}}\begin{pmatrix} e^{j\frac{(n_{eff,x_1}-n_{eff,y_1})k_0\mathrm{L}_1 t}{2}} & 0 \\ 0 & e^{-j\frac{(n_{eff,x_1}-n_{eff,y_1})k_0\mathrm{L}_1 t}{2}} \end{pmatrix} \quad \textbf{(3.1.4.14)}$$

Which is equivalent to:

$$\mathrm{T}(\mathrm{L}_1) = e^{j\frac{\Delta\beta\mathrm{L}_1}{2}}\begin{pmatrix} e^{-j\frac{\Delta\beta\mathrm{L}_1}{2}} & 0 \\ 0 & e^{j\frac{\Delta\beta\mathrm{L}_1}{2}} \end{pmatrix} \quad \textbf{(3.1.4.15)}$$

For sake of simplicity $e^{j\frac{\Delta\beta k_0\mathrm{L}_1}{2}}$ is neglected.

In order to evaluate the impact that the rotation of an alpha on the reference axes angle has on the electrical field's components, it is advisable to refer to the ideal case (x,y); for this purpose the inverse of the R matrix needs to be introduced.

$$\vec{E}_{out}(\mathrm{L}_1)=R^{-1}x\ \vec{E}_{out,1}(\mathrm{L}_1) \qquad \textbf{(3.1.4.16)}$$

By expanding $\vec{E}_{out}(\mathrm{L}_1)$:

$$\vec{E}_{out}(\mathrm{L}_1)=R^{-1}x\ \mathrm{T}(\mathrm{L}_1)x\ \mathrm{R}\ x\ \vec{E}_{in} \qquad \textbf{(3.1.4.17)}$$

$$\vec{E}_{out}(\mathrm{L}_1)=\begin{pmatrix} cos\alpha_1 & -sin\alpha_1 \\ sin\alpha_1 & cos\alpha_1 \end{pmatrix}\begin{pmatrix} e^{-j\frac{\Delta\beta k_0 \mathrm{L}_1}{2}} & 0 \\ 0 & e^{j\frac{\Delta\beta k_0 \mathrm{L}_1}{2}} \end{pmatrix}\begin{pmatrix} cos\alpha_1 & sin\alpha_1 \\ -sin\alpha_1 & cos\alpha_1 \end{pmatrix}\begin{pmatrix} E_{x,in}(0) \\ E_{y,in}(0) \end{pmatrix}$$

All mathematical passages are not reported in order to avoid burdening the discussion, the achieved result is:

$$\vec{E}_{out}(\mathrm{L}_1)\ =\begin{pmatrix} cos(\frac{\Delta\beta \mathrm{L}_1}{2})\ -\ \mathrm{j}sin(\frac{\Delta\beta \mathrm{L}_1}{2})cos\alpha_1 & -\mathrm{j}sin(\frac{\Delta\beta \mathrm{L}_1}{2})sin(2\alpha_1) \\ -\mathrm{j}sin(\frac{\Delta\beta \mathrm{L}_1}{2})sin(2\alpha_1) & cos(\frac{\Delta\beta \mathrm{L}_1}{2})+\mathrm{j}sin(\frac{\Delta\beta \mathrm{L}_1}{2})cos\alpha_1 \end{pmatrix}\begin{pmatrix} E_{x,in}(0) \\ E_{y,in}(0) \end{pmatrix}$$

Finally, is possible to express:

$$\vec{E}_{out}(\mathrm{L}_1) = E_{x,out}(\mathrm{L}_1)\,\hat{x}_1 + E_{y,out}(\mathrm{L}_1)\,\hat{y}_1 \qquad \textbf{(3.1.4.18)}$$

Where dealing with the first assumption the polarized component along x axes is 0, which bring to the following conclusion:

$$E_{x,out}(\mathrm{L}_1) = -jE_y\, sin(\tfrac{\Delta\beta \mathrm{L}_1}{2})sin(2\alpha_1) \qquad \textbf{(3.1.4.19)}$$

$$E_{y,out}(\mathrm{L}_1) = E_y\,(cos(\tfrac{\Delta\beta \mathrm{L}_1}{2}) + \mathrm{j}sin(\tfrac{\Delta\beta \mathrm{L}_1}{2})\, cos(2\alpha_1)) \qquad \textbf{(3.1.4.20)}$$

3.1.5 Optical power exchange between modes

In general terms $E_{x,in}(0)$ is different from zero, as consequence x and y polarized output fields are:

$$E_{x,out}(\mathrm{L}_1) = E_x(cos(\tfrac{\Delta\beta \mathrm{L}_1}{2}) + jsin(\tfrac{\Delta\beta \mathrm{L}_1}{2})cos(2\alpha_1)) - jE_y\, sin(\tfrac{\Delta\beta \mathrm{L}_1}{2})sin(2\alpha_1) \qquad \textbf{(3.1.5.1)}$$

$$E_{y,out}(\mathrm{L}_1) = E_y\,(cos(\tfrac{\Delta\beta \mathrm{L}_1}{2}) + \mathrm{j}sin(\tfrac{\Delta\beta \mathrm{L}_1}{2})\, cos(2\alpha_1)) - jE_x sin(\tfrac{\Delta\beta \mathrm{L}_1}{2})\, sin(2\alpha_1) \qquad \textbf{(3.1.5.2)}$$

From the Poynting's law is known that the energy flux density associated with an electromagnetic wave is defined by the following equation:

$$\mathrm{S} = \frac{|E|^2}{\mu} \qquad \textbf{(3.1.5.3)}$$

Where μ represents the magnetic permeability of the medium in which waves propagates and $|E|^2$ is the electric field's square magnitude.
Dealing to Poynting's law, the optical power, which passes through an area A, can be computed:

$$P_{opt} = \text{S x A} = \frac{|E|^2 x\ A}{\mu} \quad \textbf{(3.1.5.4)}$$

It's clear how P_{opt} is proportional to the electric field's square magnitude.
Thanks to the previous definition is possible to assess the difference of x and y polarized output optical powers respect to input ones.
The total optical output power is:

$$P_{opt,out} = P_{opt,out,x} + P_{opt,out,y} = \left|E_{x,out}(\mathrm{L_1})\right|^2 + \left|E_{y,out}(\mathrm{L_1})\right|^2 \quad \textbf{(3.1.5.5)}$$

$$P_{opt,in} = P_{opt,in,x} + P_{opt,in,y} = \left|E_{x,in}(0)\right|^2 + \left|E_{y,in}(0)\right|^2 = |E_x|^2 + \left|E_y\right|^2 \quad \textbf{(3.1.5.6)}$$

The focus is put on $P_{opt,out}$'s terms:

$$\left|E_{x,out}(\mathrm{L_1})\right|^2 = \left|E_x(cos(\tfrac{\Delta\beta \mathrm{L_1}}{2}) + jsin(\tfrac{\Delta\beta \mathrm{L_1}}{2})cos(2\alpha_1))\ - jE_y\ sin(\tfrac{\Delta\beta \mathrm{L_1}}{2})sin(2\alpha_1)\right|^2 \quad \textbf{(3.1.5.7)}$$

$$\left|E_{y,out}(\mathrm{L_1})\right|^2 = \left|E_y\ (cos(\tfrac{\Delta\beta \mathrm{L_1}}{2})\ + \mathrm{j}sin(\tfrac{\Delta\beta \mathrm{L_1}}{2})\ cos(2\alpha_1)) - jE_x sin(\tfrac{\Delta\beta \mathrm{L_1}}{2})\ sin(2\alpha_1)\right|^2 \quad \textbf{(3.1.5.8)}$$

The mathematical passages are omitted from the discussion to make it more concise; in fact, even without the development of the upper equations, is underline that an exchange of optical power along the two polarized direction happened during the propagation.
The optical power exchange is another effect to take in account when birefringent medium is on stage.

3.1.6 Beats length

In previous subparagraph, the perturbation that was mentioned, usually cause the occurrence of linear birefringence. This means that the fiber has two waveguide modes which are polarized in a linear manner and their electric field vectors are parallel to the fiber's symmetry axes.
For example, if linearly polarized input wave is launched into a short fiber at a 45° angle to the birefringent axes, the polarization state will undergo cyclic changes as the wave travels along the fiber. This means that the polarization state will change from linear to elliptical, circular, and then back to elliptical before returning to a linear state that is perpendicular to the initial state of polarization.
The output polarization state from a short birefringent fiber will undergo the same cyclic changes, moving through the various polarization states in a similar fashion, if the frequency of the light is changed while keeping the input polarization state constant.
By combining the differential index and the optical wavelength, it is possible to establish the beat length:

$$L_{beat} = \frac{\lambda}{\Delta n_{eff}} \qquad \textbf{(3.1.6.1)}$$

The meaning of the previous definition corresponds to the distance over which the polarization rotates by a complete cycle (2π phase difference accumulates between two modes of the fiber).

3.2 DIFFERENTIAL GROUP DELAY

3.2.1 DGD INTRODUCTION

For a short section of fiber of length L_1, $\Delta\tau$ is defined as the differential group delay (DGD) obtained from the angular frequency derivative of $\Delta\beta$:

$$\Delta\tau = \frac{d\Delta\beta}{d\omega} L_1 = \frac{d(\Delta n_{eff}\frac{c}{\omega})}{d\omega} L_1 = (\frac{\Delta n_{eff}}{c} + \frac{\omega}{c}\frac{d\Delta n_{eff}}{d\omega}) L_1 \quad \textbf{(3.2.1)}$$

The effective meaning of DGD is expressed through the help of the following figure.

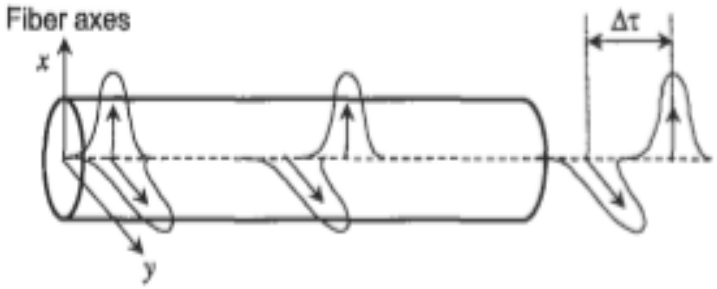

Figure 3.2.1: from chapter 15, section 2.2 of "Kaminow - Optical Fiber Telecommunications IVB - System and Impairments"

A pulse launched with equal power on both birefringent axes results in two pulses at the output, separated by the DGD, as shown in Figure 1.2, which illustrates the effect in a short fiber[6].

3.2.2 DGD STATISTICS

In the short-length regime, DGD is deterministic because the birefringence has a simple additive effect. However, in modern transmission systems, fiber lengths are much longer, spanning hundreds or thousands of kilometers. In these systems, the birefringence is not strictly additive, as there are random variations in the orientation of the birefringent axes along the fiber length. This can cause a phenomenon known as polarization-mode coupling, where the polarization modes ($LP_{01,x_{i-1}}, LP_{01,y_{i-1}}$) from one segment, whose depend on $n_{eff,x}$ and $n_{eff,y}$, can split into both LP_{01,x_i} and LP_{01,y_i} modes of the next segment.

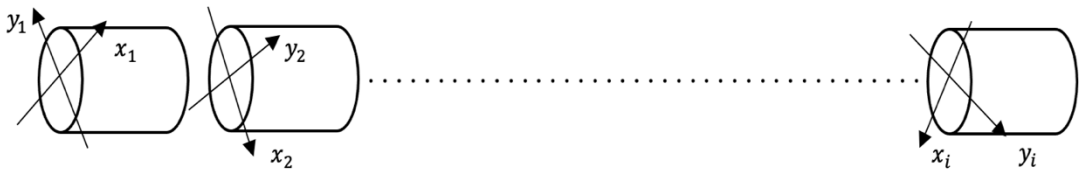

Figure 3.2.2

According to Figure 3.2.2, long fiber can be split in different birefringent sections, whose birefringent axes change randomly in each one.

The DGD does not increase linearly with fiber length, because of mode coupling, which allows each section's birefringence to either increase or decrease the total birefringence. Indeed, it has been demonstrated in long fiber spans, that on average, the DGD value rises with the square root of distance (Poole 1988a; Poole and Nagel 1997). Although mode coupling adjusts the DGD of a fiber span, for instance, variations in external stresses will change the mode coupling and subsequently the fiber's DGD. Because the mode coupling depends on the fiber's environment, that is unpredictable, possible to treat the statement with statistical tools.

The correlation length L_{seg}, also known as the coupling length, is a parameter that determines whether a fiber belongs in the short or long length regime (Kaminow 1981). This parameter describes the equivalent random coupling between the two polarization modes of a fiber with principally uniform birefringence subject to random perturbations or the weak random coupling among two waveguides.
It considers the length dependent evolution of the polarizations in a set of fibers with statistically equivalent perturbations.
L_{seg} and L_b are linked with the DGD by means of variance:

$$\sigma_\tau{}^2 = <\Delta\tau^2> = 2\left(\frac{\lambda}{c}\frac{L_{seg}}{L_{beat}}\right)^2\left(\frac{L}{L_{seg}} + e^{-\frac{L}{L_{seg}}} - 1\right) \qquad \textbf{(3.2.2.1)}$$

The formula is derived from the statistical theory of PMD[7] and it holds for both short length fiber and long length fiber regimes.

It follows the demonstration of this framework:

1. Short length regime: L<< L_{seg}

   Thus, the DGD standard deviation in this case is:

$$\sigma_\tau = \sqrt{<\Delta\tau^2>} = \Delta\tau_{rms} = \frac{\lambda}{c}\frac{L_{seg}}{L_b} \qquad \textbf{(3.2.2.2)}$$

   It is possible to notice how σ_τ increases or decreases linearly with L_{seg}.

2. Long length regime: L >> L_{seg}

   In this scenario, the DGD standard deviation increases or decreases according to square root of distance, the result is[9]:

$$\sigma_\tau = \sqrt{<\Delta\tau^2>} = \Delta\tau_{rms} = \frac{\lambda}{c}\frac{1}{L_b}\sqrt{2LL_{seg}} \qquad \textbf{(3.2.2.3)}$$

Hence is possible to assess the evolution of σ_τ against $\sqrt{L}$:

$$\frac{\sigma_\tau}{\sqrt{L}} = \frac{\Delta\tau_{rms}}{\sqrt{L}} = \frac{\lambda}{c}\frac{1}{L_b}\sqrt{2L_{seg}} \qquad [\frac{\text{ps}}{\sqrt{Km}}] \qquad \textbf{(3.2.2.4)}$$

3.3 POLARIZED MODE DISPERSION (PMD)

3.3.1 First order PMD definition

In subparagraph 3.1.2 was provided the group velocity definition. It depends on the $n_{eff,x}$ and $n_{eff,y}$.

If a short length fiber is considered, the electric field propagating in z direction, decomposes into a x and y polarized electric fields.

As already discussed, they propagate through birefringent medium, which means that during the propagation they accumulate certain optical phase shift and differential group delay (DGD is proportional to the fiber's length).

Since $n_{eff,x}$ and $n_{eff,y}$ are different, one is larger respect the other; this consideration leads to take in account that the group velocity of one mode is faster than the other. At this purpose, for convention $n_{eff,x}$ and $n_{eff,y}$ will be called, respectively, n_{fast} and n_{slow}.

The goal of following figure is to explain from visual point of view the framework introduce so far, in presence of non-ideal core.

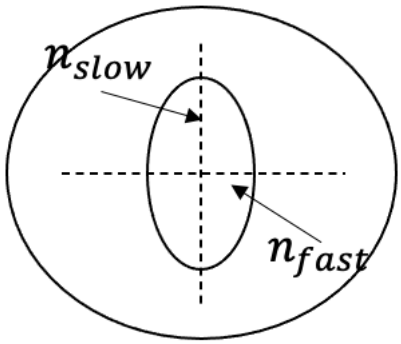

Figure 3.3.1

DGD together with polarization states are the fundamental roots of first order PMD. There are two ways to describe the polarization mode dispersion of a randomly mode-coupled span:

- Instantaneous DGD is defined when DGD is considered at a given wavelength and at given time.
- PMD delay is defined when the average of DGD over wavelength is considered. With this definition is possible to derive the PMD coefficient D_{PMD} :

$$D_{PMD} = \frac{\sqrt{<\Delta\tau^2>}}{\sqrt{L}} \qquad [\frac{psec}{\sqrt{km}}] \tag{3.3.1}$$

D_{PMD} represents the ratio between average DGD and the fiber length square root. D_{PMD} typical values span onto range [0,1; 0,2][9].

3.3.2 Principal State of Polarization

PMD, more than just the nature of the differential group delay, is impacted by the presence of mode coupling; the fast and slow polarization modes also adopt elliptical states and change with wavelength and time. However, there exists an orthogonal pair of states at the fiber's input that correspond to early and late arrival of energy at the fiber's output at any given wavelength and time in the absence of polarization-dependent loss.

The *principal states of polarization* (PSPs) are the definitions that characterize these special input states. Another pair of principal states are at the fiber path's output.

The PSPs are the result both mode couplings that form the fiber path and birefringence's random configuration; any variations in these outlines corresponds to PSPs shift, which leads to the conclusion that the input and corresponding output PSPs are different.

An input/output principal state pair, for instance the input and output fast polarization modes, can be distinguished by the fact that the transition between these two states is wavelength independent over a suitably small wavelength range. The PSP bandwidth is the narrow frequency range's average value (over wavelength), over which PSPs exhibit frequency independence.

Both the differential group delay and the PSPs vary across the signal spectrum when the spectral width of the signal is greater than the PSP bandwidth. Higher order PMD effects result from this, including chromatic dispersion and a pulse distortion caused by a change in the primary states of polarization throughout the pulse spectrum.

First-order PMD's effects on an operating link depend on the relative intensities of light in the principal states of polarization as well as the differential group delay. When all the light is coupled to one principal state of polarization, the impairment is minimal, and it is greatest when equal amounts of light are coupled into each of the input principal states of polarization.

Chapter 4

Within this chapter will be provided a numerical software developed with MATLAB.
The program will consider temperature changes, consequently the birefringence coefficient will depend on different temperature values measured in different interval of time; in other words, there is time varying behaviors of $|E_{out,x,1.27}|$, $|E_{out,y,1.27}|$ and $|E_{out,x,1.33}|$, $|E_{out,y,1.33}|$.
The effects due by temperature are the principal cause of the fluctuations of total power on the λ_2 and λ_1 behaviors (already reported in Figure 1.3).
The software aims to simulate the polarization-related phenomena (the unpredictable fluctuations on $\lambda_2$and λ_1) of the SKA-Low RFoF receiver, by taking as input different temperature measurements taking on MRO's site.

4.1 Code description

To reproduce with high fidelity the real case, within code a fiber with total length (L_{tot}) of 5350 meters is considered. Furthermore, this fiber is split in span (L_{span}) of 10 meters each.

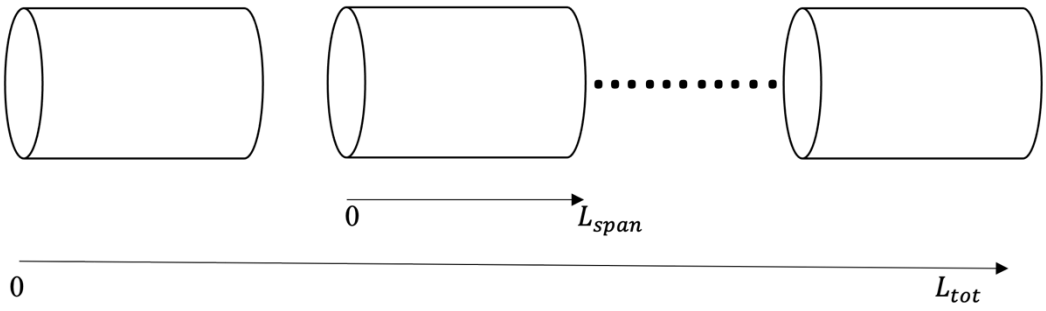

Figure 3.1 Illustration of optical fiber considered in numerical model; it is composed by 523 spans.

The temperature variations cause extrinsic perturbations on the optical fiber, so that each fiber's span undergone either dilatations or contractions. This means that, as known by theory, the fields components that propagate through the fiber spans are polarized

according with reference systems rotating by angle $\propto_i$ (i=1…..N), with respect to the original one.

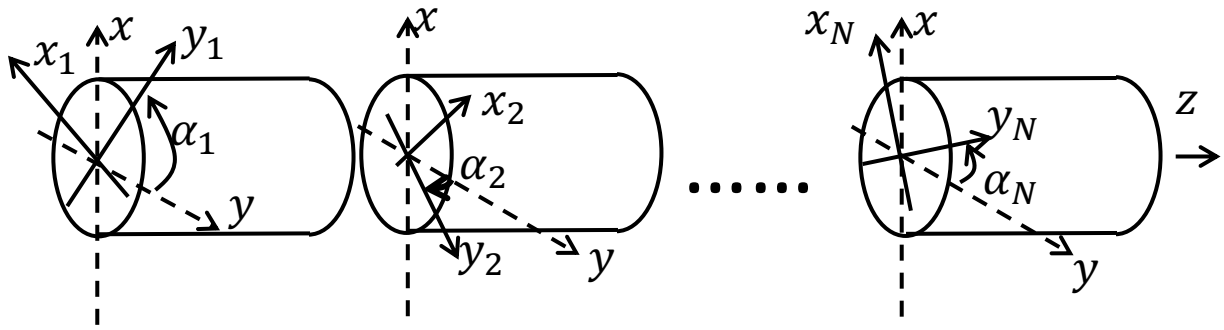

Figure 3.1.1

To define the field at the output of each span the matrices, already introduced in subparagraph 3.1.4, are defined and computed within code.

$$\bar{E}_{\lambda_k,out}(L_{span}) = R^{-1}\text{x}\left(T_{\lambda_k}\text{x}\left(\text{R x }\bar{E}_{\lambda_k,in}(L_{span-1})\right)\right) \qquad \textbf{(4.1.1)}$$

Note: the output field will depend also on the wavelength considered (λ_1 or λ_2).

Actually, the Jones matrix in code is not totally equal to the one defined before, because this time the birefringent coefficient depends on temperature.

$$T_{\lambda_i} = \begin{pmatrix} e^{j\frac{\Delta n(T(t))k_0 L_{span}}{2}} & 0 \\ 0 & e^{-j\frac{\Delta n(T(t))k_0 L_{span}}{2}} \end{pmatrix} \quad (\text{i=1,2}) \qquad \textbf{(4.1.2)}$$

In fact, the code, during one of the first iterations import the temperature files.
These files contain the optical fiber's observations within interval of 72 hours; the total interval is subdivided again in shorter interval of time and within each one of them a

different value of temperature is considered. The temperature value on all the fiber length for each time interval is supposed to be constant.

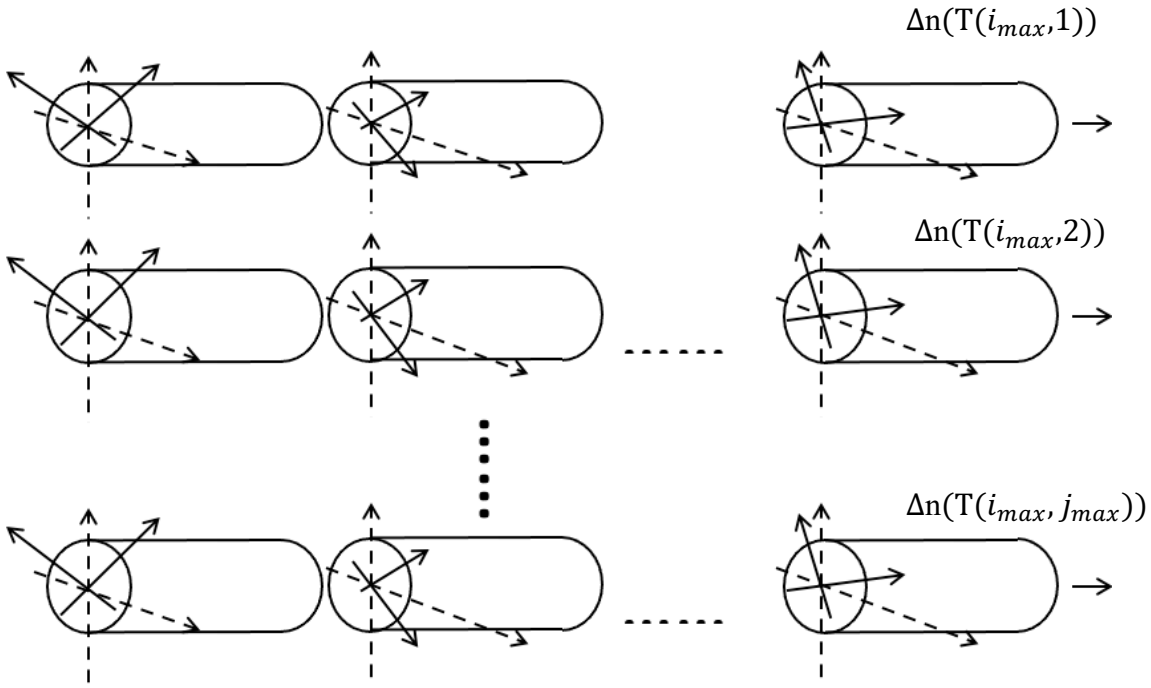

Figure 4.1.2

From Figure 4.1.2 is possible to see how the first birefringence coefficient Δn*(T(i,1),* with i that goes from 1 to i_{max} (in this case i_{max} =523) and it depends on the first time interval temperature value, will be different respect the last one, that depends on the j-th time interval temperature value. Instead, the alpha angles are the same for each fibers.
At this purpose, the script provides a parameter, which measures the birefringence coefficient in each time interval:

$$\Delta n = \Delta n_{T_0} + \frac{d(\Delta n)}{dT}\Delta T \qquad \textbf{(4.1.3)}$$

By considering the Jones matrix and by substituting the equation to its exponents, it is obtained:

$$\gamma_i = \frac{\Delta n k_0 L}{2}\Big|_{T_o+\Delta T} = \frac{\Delta n k_0 L}{2}\Big|_{T_o} + k_0 \frac{d}{dT}\left(\frac{\Delta n * L}{2}\right)\Delta T \qquad \textbf{(4.1.4)}$$

Where Δn, T_0, $\frac{d(\Delta n * L)\Delta T}{dT}$ are defined in the code with values that are taken from literature.

From which by considering only Δn:

$$\frac{\Delta n}{2}\Big|_{T_o+\Delta T} = \frac{\Delta n}{2}\Big|_{T_o} + \left[\frac{d}{dT}\left(\frac{\Delta n}{2}\right) + \frac{\Delta n}{2}\frac{1}{L}\frac{dL}{dT}\right]\Delta T \qquad \textbf{(4.1.5)}$$

$\frac{\Delta n}{2}\Big|_{T_o}$ represents the value of coefficient value of birefringence in case the temperature was constant in each time interval, in other hands $\left[\frac{d}{dT}\left(\frac{\Delta n}{2}\right) + \frac{\Delta n}{2}\frac{1}{L}\frac{dL}{dT}\right]\Delta T$ depends on the different temperatures in each time interval.

This is how the different matrices and input and output fields of each span are defined in the code.

For their calculation in each fiber span and considering different temperature values in different time intervals, two *for loops* are inserted, one dependent on i and the other on j. In this way the (3.1.4.17) becomes:

$$\bar{\bar{E}}_{\lambda_k,out}(L_{span})(i,j) = R^{-1} \text{x} \left(T_{\lambda_k} \text{x} \left(R \text{ x } \bar{\bar{E}}_{\lambda_k,in}(L_{span-1}(i,j)) \right) \right) \qquad \textbf{(4.1.6)}$$

Since the aims of the code is to also simulate the optical receiver polarization dependent effects, the PDL must be considered.

For this reason, the fields in the last spans are considered, as it is reported in Figure 3.1.3.

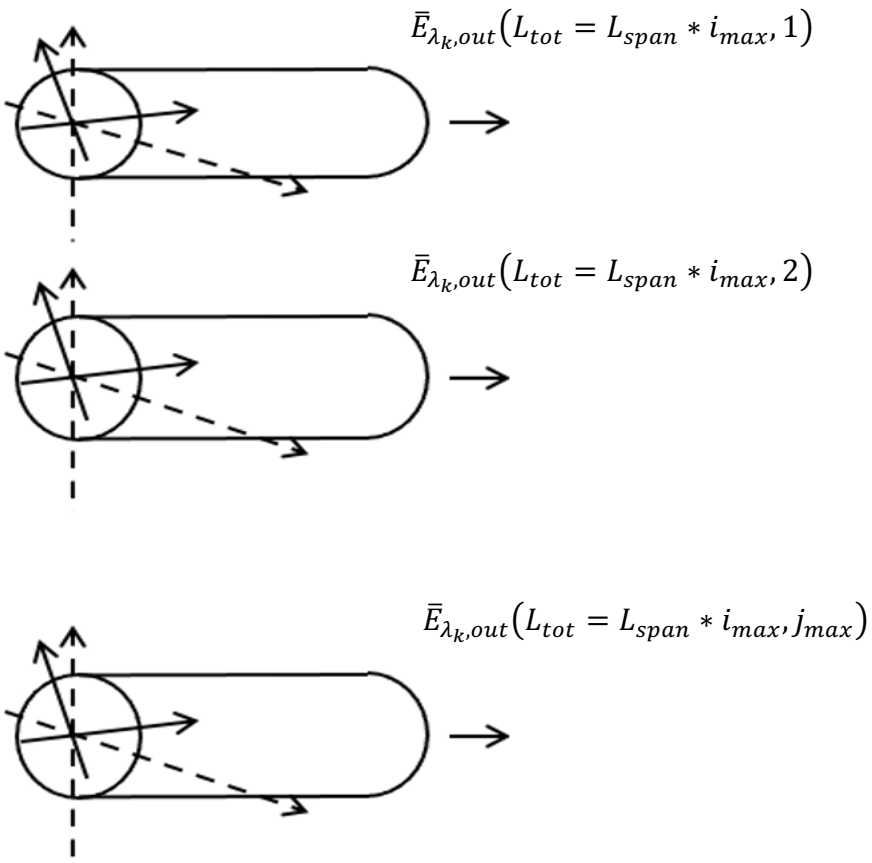

Figure 4.1.3

Then is defined the PDL matrices W_{λ_k} ,for both the polarizations, in the way already discussed in the 2.1 paragraph.

The PDL coefficient for λ_1 or λ_2 are defined in the code with a certain value based on the one measured on the type of BOSA utilized, and in particular on the specific TFF;

for example, if SSopt PREADU are utilized, two possible PDL coefficients values can be 0.13 for λ_2 and 0.6 for λ_1 (those are the median values taken by the sperimental measurements done and described in subparagraph 2.3.3).

The output field, which is reflected or transmitted by the optical receiver is due by:

$$\bar{E}_{\lambda_k,out}(L_{span}{*}i_{max+1}, \text{j}) = W_{\lambda_k} \text{ x } R^{-1}\text{x } (\ T_{\lambda_k}\text{x } (\text{R x } \bar{E}_{\lambda_k,out}(L_{span} * i_{max+1}, \text{j}))) \quad \textbf{(4.1.7)}$$

4.2 Simulations results

The task was to simulate fluctuations on λ_1 and λ_2 by exploiting the median PDL values obtained from the statistic on the SSopt's BOSA (2.3.3 subparagraph). To do that, the following results are achieved by setting those parameters:

- $L_{span} = 10$ (m)
- $L_{\text{tot}} = 5320$ (m)
- λ_2 = 1330 nm
- λ_1= 1270 nm
- $\frac{d}{dT}(\Delta n) = \frac{\Delta n}{139.34}$
- $\frac{1}{L}\frac{dL}{dT}$=5*10^-7
- Time = 72 h

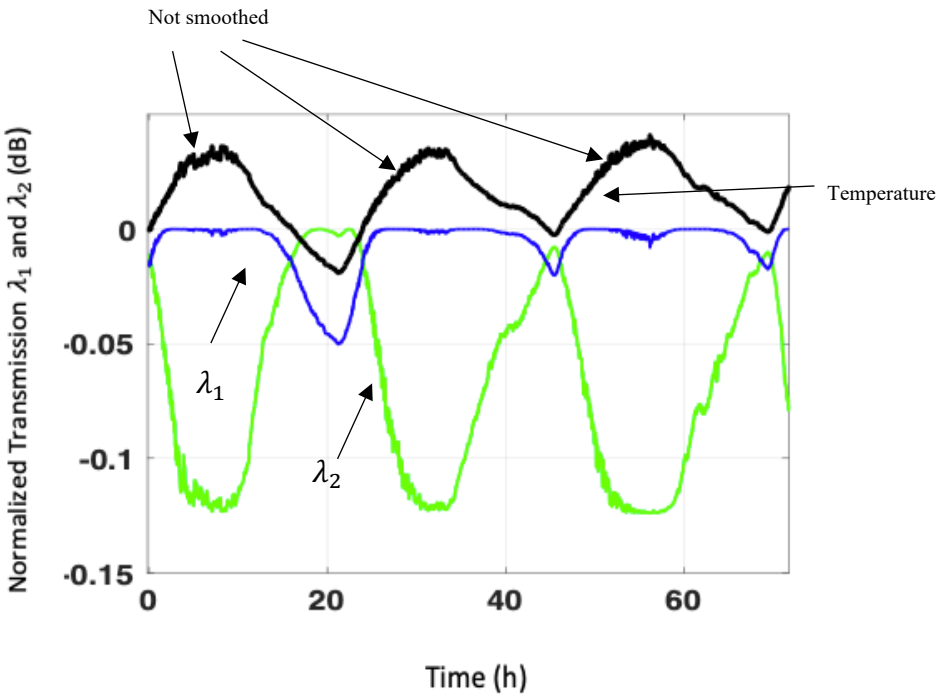

Figure 4.2 On the ordinate the normalized λ_2 and λ_1 powers are reported. On the abscissa there are the 3 days (72 hours) at which the temperature measurements on MRO site are taken. The black curve reports the temperature variations.

The two normalized powers show same time evolution, so that opposite and correlated behaviors. This first result corresponds to the one obtained with the Mickey Mouse manual controller in Figure 2.2.2.

Then, it is possible to realize that with the PDL median values collected by the Ssopt, on λ_1 the fluctuations are present, when the temperature is at its peak and they are minimal respect to ones observed on λ_2.

Moreover, it is clear from the picture, how the fluctuations on λ_2 appear also when during the day, temperature starts to be high and when it starts to decrease.

Chapter 5

The previous chapter was dedicated to the presentation of the software that allows to simulate the fluctuations on the $\lambda_1$and λ_2 normalized powers, receiving as input both a certain set of parameters and temperature values measured for a period (usually days).
However, as already disclosed in paragraph 1.3, the fluctuations are the result of the combination of the effects of PDL and PMD (where the PMD is a value known from the fiber'sstandards).
This assumes that the correct functioning of the software must be verified by an "alpha" test.
In other words, a MATLAB software has been developed which, having received input data relating to the polarization angles of the input fields, segment length, beat length, phase shift of the field components and wavelength, verifies that the DGD standard deviation grows as the root of the total length of the fiber.
The real goal is to obtain the length of the segments and beats starting from the std DGD value (and therefore, as seen in the paragraph 3.3, from the PMD value).
The formula (3.2.2.4) is reported to make clearer the previous framework:

known $\rightarrow$ $\frac{\sigma_\tau}{\sqrt{L}} = \frac{\lambda}{c}\frac{1}{L_b}\sqrt{2L_{seg}}$ $\leftarrow$ unknown

5.1 Code description

In the following, a block diagram is introduced to explain basic principles on which its operation is based.

Vector and parameters initialization:

λ = 1270 (or 1330) 10^{-9}
$f_1 = \frac{c}{\lambda}$ (speed of light)
delta_f = *10*
$f_2 = f_1$ + delta_f
L_beat_vector = π ∗[1,2,4,16,32] (length of beats)
L_segment_vector = [20,30,40,60] (fiber span's length)
chi_start_vector = 0: $\frac{\pi}{120} : \frac{\pi}{2}$ (it represents all possible polarizations angles of the field's components at the input of the first segment)
delta_start_vector =- $\frac{\pi}{2} : \frac{\pi}{120} : \frac{\pi}{2}$ (it all possible phase displacement angles of the field's components at the input of the first segment)
i_vector=20:20:1000 (Number of segments constituting the different spans considered)
j_max=100 (The index "j" indicates the trials , the number of fibers, with different alpha vectors for each spans)
Biref=$\frac{\lambda}{L\_beat\_vector}$

Three executions of the program are pursued:

a. By fixing chi_start_vector = 0 or $\frac{\pi}{4}$ and delta_start_vector = 0 (it means orthogonal polarization of the field's components generated by lasers).
b. By fixing L_beat_vector= π*32 m, L_segment_vector=60 m and delta_start_vector=0.
c. By fixing L_beat_vector= π*32 m, L_segment_vector=60 m and chi_start_vector=0.

5.1.1 Executions description

chi_start_vector =0 or $\frac{\pi}{4}$

delta_start_vector = 0

```
for i_beat = 1:length(L_beat_vector)
    for i_segment = 1:length(L_segment_vector)
        for i_length=i:length(i_vector)
```

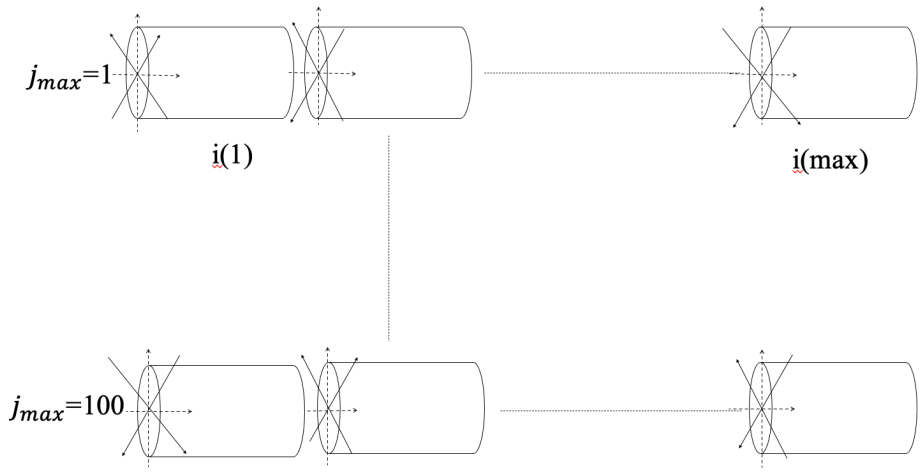

Figure 5.1.1 It is reported the in a graphical way what for loops done.At each i iteration the number of segments increases until reach its maximum that is 1000.J number hold for the number of fibers considered, which have the same number of i.At each L_seg cycles, the segment length increases until reach its maximum values (60).

At the end of all the cycles the total fiber lengths is of 60 Km (60*1000) and the beat length of 32* π m.

Inside the internal cycle (the i one) the computation of the output field at each sections happen by implementing the (3.1.4.17).

It follows the computation of the group delay $\tau_{g,x}$(j,i) and $\tau_{g,y}(j,i)$ for both polarized components and for each j and i.

With that the DGD(j,i), which gradually accumulates at the end of each section (on each j fiber).

Once all cycles are completed, the final DGD is calculated for each j, but for the maximum value of i (1000 of segments).

The final count is the DGD standard deviation (σ_τ=std(DGD_total_final)).
The mean value is not computed because it is 0, since some components in some sections are faster respect to the other, in other sections, it may happens the opposite, at the end there is a sort of compensation effect.
The other two executions show the same logic, but:

- b

  L_beat_vector = 32* π

  L_segment_vector = 60

  delta_start_vector = 0

  for i_chi = 1:length(chi_start_vector)
  for i_length=i:length(i_vector)

- c

  L_beat_vector = 32* π

  L_segment_vector = 60

  chi_start_vector = 0

  for i_delta = 1:length(delta_start_vector)
  for i_length=i:length(i_vector)

5.2 Results

5.2.1 Analytical and numerical results

Before proceeding with the software results, it is important to clarify that in the script just presented, no analytical formula for calculating the DGD standard deviation has been implemented.
Hence, it is appropriate to demonstrate that the results obtained numerically faithfully reflect the analytical trend.
Therefore, a script implementing the (3.2.2.1) and (3.2.2.3) has been developed.
The results obtained, by setting L_segment_vector to 60, L_beat_vector to 32*π and i=20:20:1000 are:

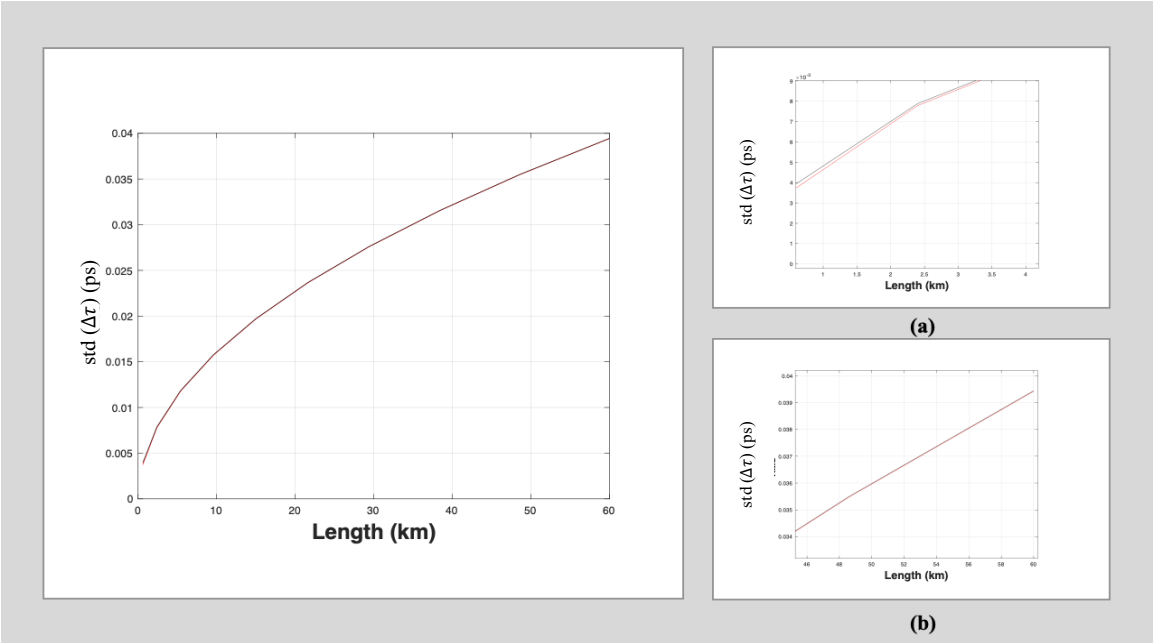

Figure 5.2.1 On the ordinate there is the DGD standard deviation expressed in ps, instead on the abscissa the total length, in Km, is reported. The curve's behavior deals with a square root shape with the increase of the length (as the long term regime holds). In (a) there is a zoom at the begging of the distance to underline that, the (3.2.2.1) and (3.2.2.3) not coincide for short distance, while they do for the long one (as reported in (b), where a zoom for higher length is done).

The DGD standard deviation against length obtained with the execution (a.) present the following result:

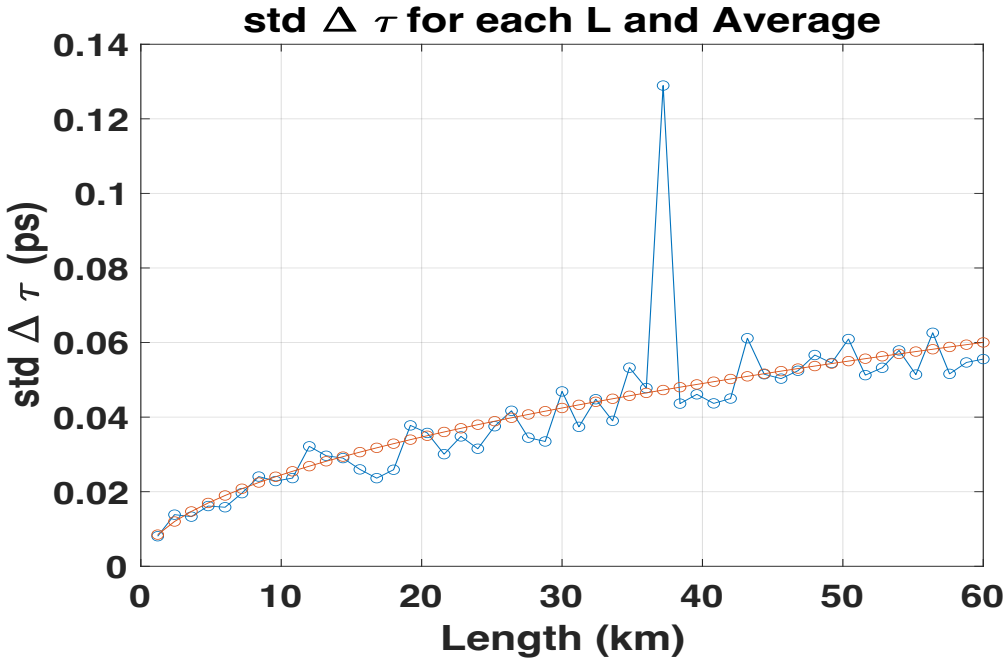

Figure 5.2.1.2 On the ordinate there is the DGD standard deviation expressed in ps, instead on the abscissa the total length, in Km, is reported. The blue dots, on the blue line, represent the standard deviation computed at the end of each segment that compose the whole optical fiber (in fact there are 50 dots). The red dots, on the red line, are the fitting, in other words describe the average increase of the standard deviation.

From Figure 5.2.1 and from 5.2.1.2 plots is clear as, the DGD std achieved numerical result shows a square root fashion, that seems respect the one obtained with the analytical one.

This is the first important result, because it demonstrates that the numerical model can be used to simulate the DGD standard deviation in different situations.

5.2.2 Execution (a.) results

Figure 5.2.2 reports the DGD standard deviation values for each segment that compose a 60 Km fiber, for a beat legth of $32*\pi\ m$ and with j=100.
At this point, since the $\frac{\sigma_\tau}{\sqrt{L}}$ (like D_{PMD}) is a specific present on the data sheet, it useful to average σ_τ on the total length (60km).

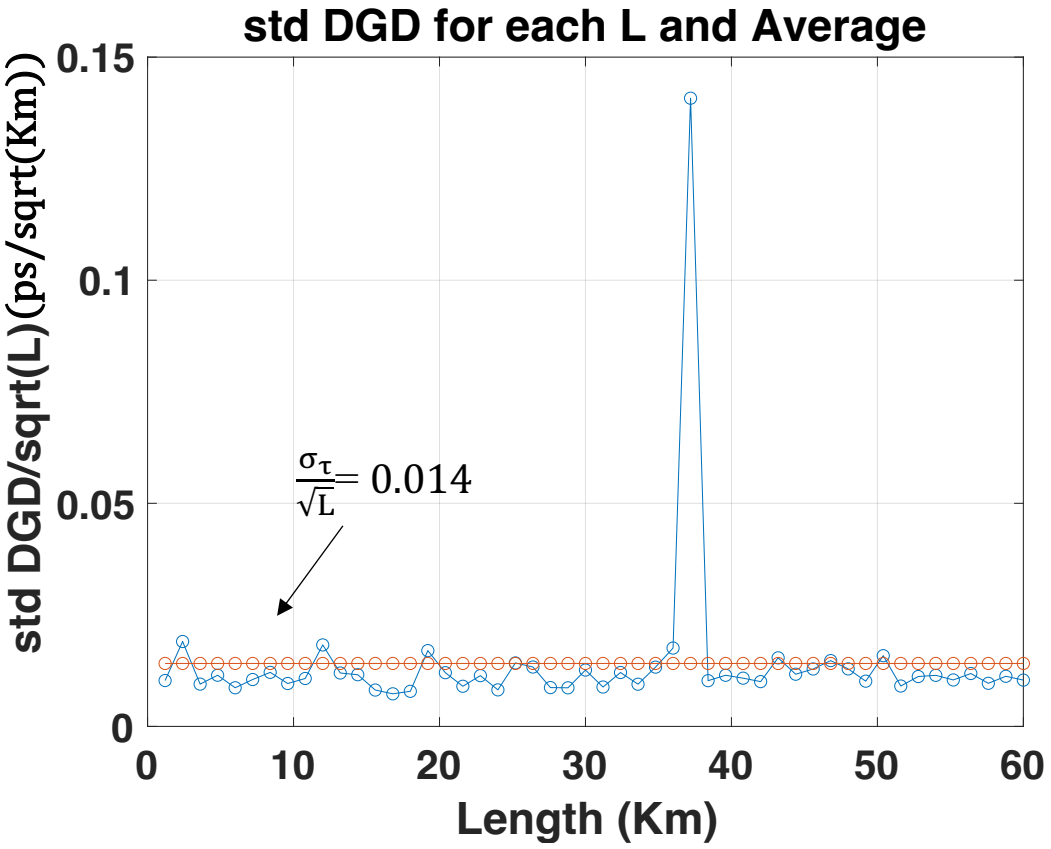

Figure 5.2.2 As expected the std DGD value is constant (red dot) against the whole length, this result is the (3.2.2.4) application.

Moreover, another practical demonstration that the numerical model is good for the std analysis is due by changing the maximum value of L_beat_vector.

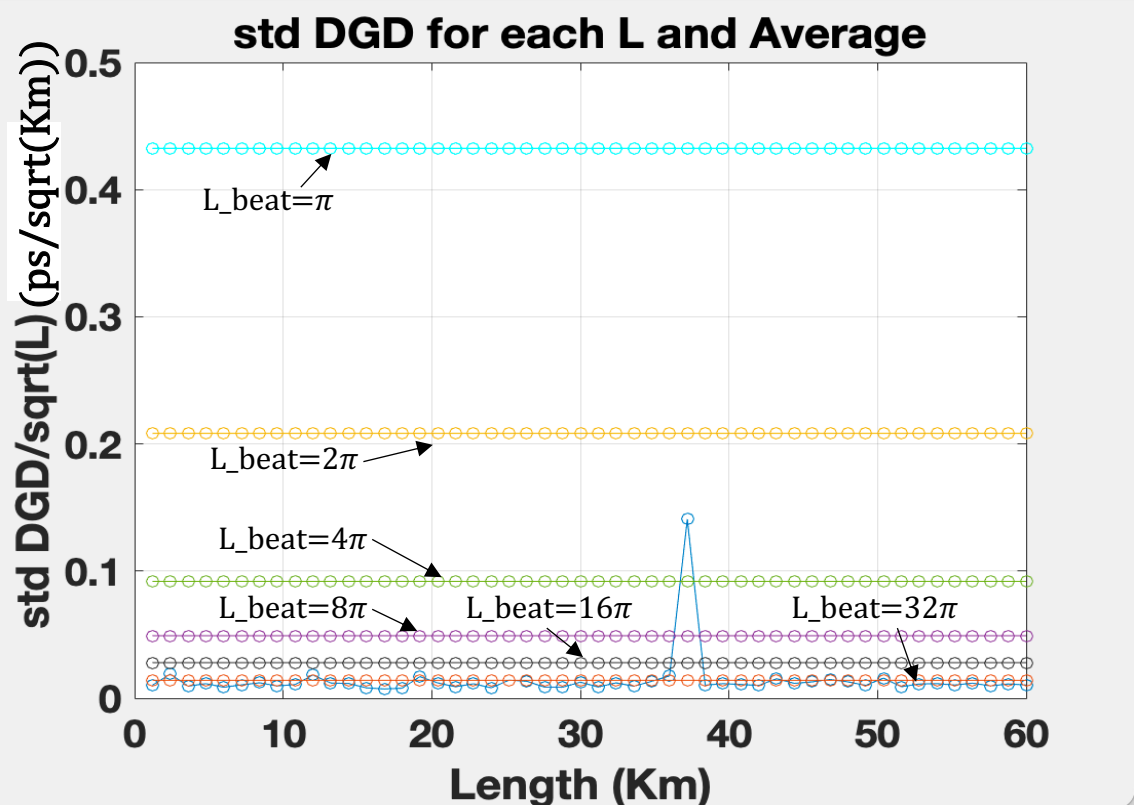

Figure 5.2.3 Figure 5.2.2 is taken as a reference. The lines with. different colors represent the different values of $\frac{\sigma_\tau}{\sqrt{L}}$ for different beat lengths.

The results obtained from figure 5.2.3 deal with (3.2.2.4), in facto for small values of beat length, that mean also larger birefringence, $\frac{\sigma_\tau}{\sqrt{L}}$ increases.

This can be considered a second important result.

The third result, with this kind of code execution, derives from the change in terms of j_max.

In fact, one trial is conducted, by considering a larger number of fibers in order to see the statistical difference with a larger number of instances.

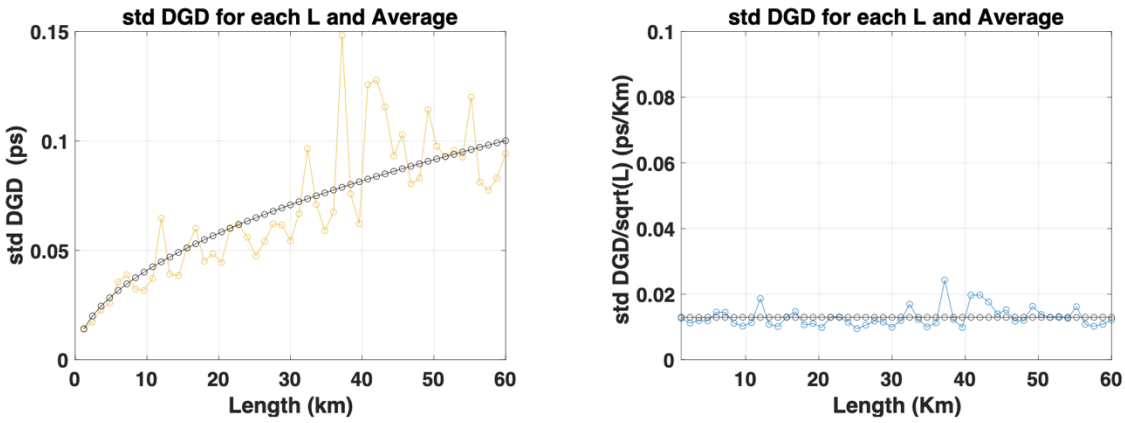

Figure 5.2.4 Those figures report the same parameters of Figure 5.2.1 and 5.2.2.

In first view, Figure 5.2.4 present, more or less, same results obtained with j_max=100.

The impression is confirmed with results superimposition.

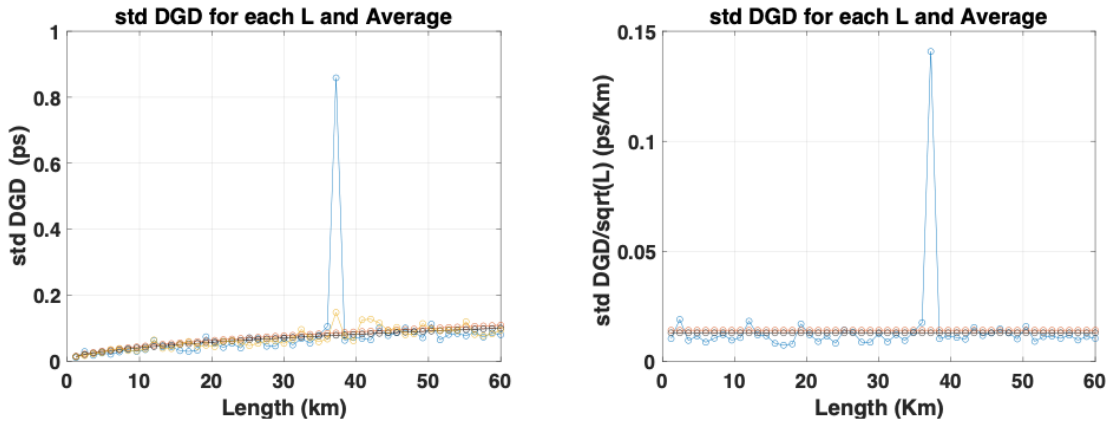

Figure 5.2.5

Figure 5.2.5 proves that even if the number of instances increases, no different std DGD values are achieved.

The third result allows to consider j_max=100, which means less heavy code.

5.2.2 Execution (b.) results

As anticized, in this execution the same script is launched, with fixed values of segment length (60), beat length (32*π) and delta start (0).

The same computations are made by changing the chi (χ) start vector, which means that different field's polarization angles at the input of the first segment are considered.

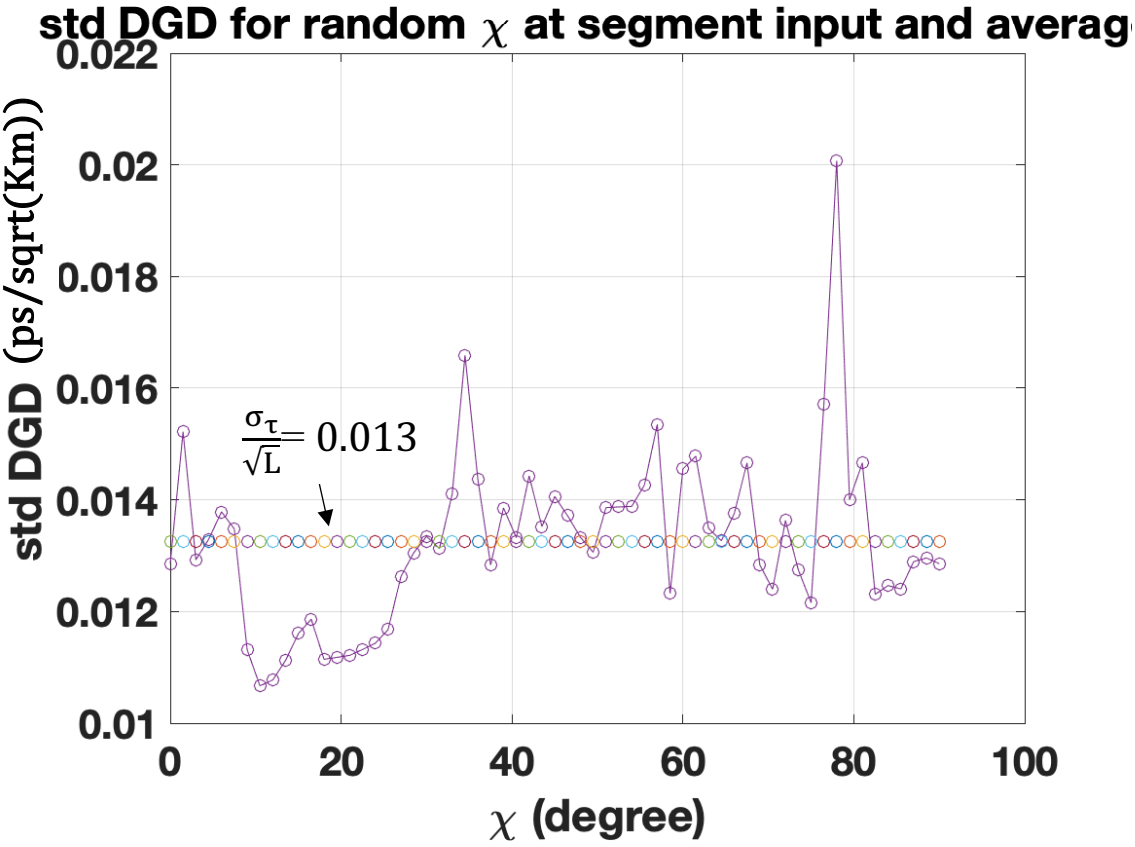

Figure 5.2.2 It is reported on the ordinate $\frac{\sigma_\tau}{\sqrt{L}}$, while in the abscissa the value of χ, that goes from 0 to $\frac{\pi}{2}$ (because the purple curve has periodicity of $\frac{\pi}{2}$).

Dealing with $\frac{\sigma_\tau}{\sqrt{L}}$ (0.013) values reported in Figure 5.2.2 and comparing it, to the one obtained from the previous code execution (the a. one, that is 0.014), it is possible to achieve the fourth result: even if the polarization's angles of fields in input in the first segment is different to 0, the final result is basically the same.

Actually it is important to say that LASER sources emit, always rectilinear polarized field's components, which means that the phase shift between components can be considered equal to 0.

5.2.3 Execution (c.) results

Last run of the script is done by considering fixed values of segment length (60), beat length (32*π) and chi start (this time set to $\frac{\pi}{4}$).

The computation is done by varying delta start, which represents the phase shift between the field's components at the input of first segment.

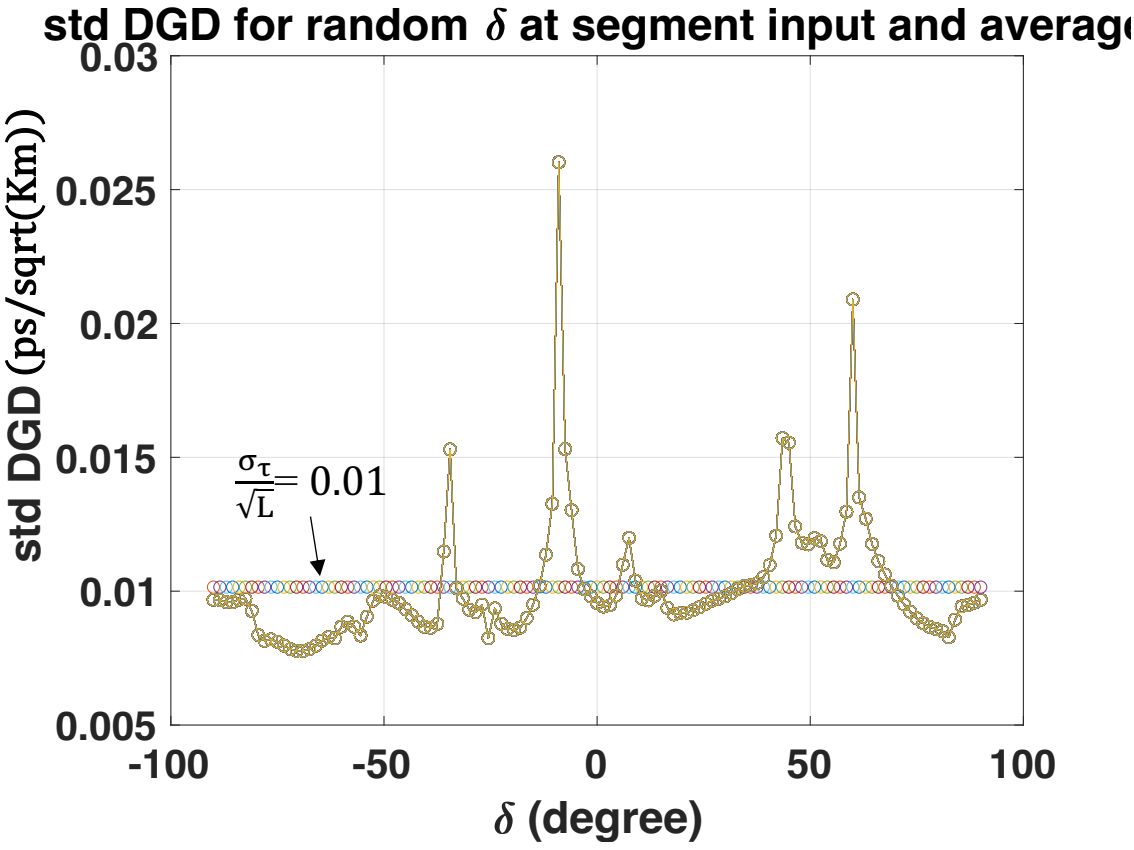

Figure 2.2.3 It is reported on the ordinate $\frac{\sigma_\tau}{\sqrt{L}}$, while in the abscissa the value of δ, that goes from $-\frac{\pi}{2}$ to $\frac{\pi}{2}$.

According to $\frac{\sigma_\tau}{\sqrt{L}}$ (0.01) result reported in Figure 5.2.3 and comparing it, to the one obtained from the previous executions (the a. one, that is 0.014 and the b. one, which is 0.013),the fifth result is found: there are phase displacement angles that minimize the $\frac{\sigma_\tau}{\sqrt{L}}$,

instead others in which $\frac{\sigma_\tau}{\sqrt{L}}$ is quite high; but on average the std DGD against square root of length is again quite similar to the previous ones.

Hence, the conclusion is that the polarization's angle components and the phase shift between field's component don't show any impact in terms of $\frac{\sigma_\tau}{\sqrt{L}}$.

Chapter 6

6.1 Conclusions

Given the harsh conditions of the Western Australian desert, the anticipated lifetime, and the low cost, RFoF for SKA-low requires considerable effort to achieve the requested RF performances.

In chapter 1, it was explain that this thesis focused mainly on the SKAlow receiver, between the demonstrators that are already used in the MRO site (AAVS2) and new versions that will be installed (AAVS3), and the analog receivers of the CPF/RPF.

In particular, the parts, of the SKAlow receiver, most taken into consideration were the BOSA WDMs mounted on the PREADU.

In chapter 3, it was explained how extrinsic perturbations of the optical fiber are the cause of the phenomena which impact on the polarization of the fields that propagate through it. These phenomena are birefringence first, hence the consequence DGD and therefore the PMD, which is the value given in the G652 standards.

The polarization dependence of BOSA WDMs is the cause of fluctuations on the received RF power.

The RF power is composed by two components RF_1 and RF_2 ,which in the optical domain are modulated, respectively, with λ_2 (1330 nm) and λ_1 (1270 nm).

In chapter 2, the PDL was treated through the example of the optical receivers (EZconn) in the PREADU used in the SKAlow receiver for AAVS2.

Finally, in the same chapter, PDL measurements carried out on new optical receivers (SSopt BOSA PD) and consequently a statistical analysis of the results has been reported to give an effective meaning to the values obtained.

The task of chapter 4 was to introduce the MATLAB software, that taking as input some parameters (e.g. the temperature measurements in different time instants, the PDL values

for RF_1 and RF_2 normalized power, the fiber length) is able to simulate the fluctuations on the RF_1 and RF_2.

The previous software has been justified by another script, which takes out simulations on DGD on one single optical fiber. In fact, with this numerical model has demonstrated what was mentioned in chapter 3 for only one fiber.

Through various tests, it was understood that the DGD standard deviation against square root of length value does not vary with the variation of the polarization angles of the input field components and their initial phase shift. Instead, it has also been proved numerically that the standard deviation has smaller values as the length i beat increases (smaller birefringence) and as the total length of the fiber increases, it grows proportionally to the square root of the length.

6.2 Ongoing activities

The focus of a future effort could be understanding how much the RF power fluctuations on the optical receivers of the various log-periodic antennas are an issue, given that they should be uncorrelated by nature; this would means that the various fluctuations due to optical receivers uncorrelation could mitigate each other.

Other options should be either investigate on BOSA PD with lesser PDL values or buried part of the optical link. This last action should allow to slow down the PMD, which means minimize the fluctuations on the RF received power. This because, the extrinsic perturbations on the fiber's core are limited, since the strong ambiental environment's phenomena have no impact.

REFERENCES

- [1]. www.skao.it – SKAmid-SKAlow.
- [2]. F.Perini et al.- "Radio frequency over fiber technology for SKA-low receiver"-Jan 2022-JATIS
- [3]. F.Perini et al.- "SKA-low and RFoF – Overview and current status"-Internal presentation-July 2022
- [4]. Prof. Giovanni Tartarini - "PDL and PMD notes" –Internal presentation-July 2022
- [5]. Articles-Polarization_Mode_Dispersion_Concepts.- www.photonics.com
- Pal Roe Sundsoy- "Depolarization of orthogonal states of polarization in fiber optic high-speed transmission"-2004-PhD Thesis Department of Physics-NTNU July 29,2004
- [7]. Poole et al.- "Statistical treatment of polarization dispersion in a single mode fiber"-1994-IEEE
- [8]. Kaminow,Li - "Optical Fiber Telecomm IVB- System and Impairments"-2002.
- [9]. Prof. Giovanni Tartarini - "Optical Fiber Systems notes".